Supplementary Information (SI) for Dalton Transactions.
This journal is © The Royal Society of Chemistry 2025

# Supplementary Information

# Dual Tuning of Nodes and Functional Guests of Polyoxometalate@Metal-Organic Frameworks for Enhanced Photocatalytic Oxidative Coupling

Zhiqiang Jiang, [a,+] Qixin Zhao, [a,+] Yang Zeng, [a] Tengfei Gong, [b] Zhenxuan Huang, [a] Zeyu Chen, [a] Jiefeng Shen, * [a] and Weimin Xuan * [a]

[a] State Key Laboratory of Advanced Fiber Materials & College of Chemistry and Chemical Engineering, Donghua University, Shanghai 201620, P. R. China. *E*-mail: jiefeng@dhu.edu.cn, weiminxuan@dhu.edu.cn

[b] Jiaxing Jiayuan Inspection Technology Service Co., Ltd, Building 2, No. 1403, Hongbo Road, Economic and Technological Development Zone, Jiaxing City, Zhejiang Province, P. R. China. *E*-mail: tengfeigong@126.com

[+] These authors contributed equally to this work.

# Contents

1. Materials ..... 3

2. Instrumentation ..... 3

3. Synthesis ..... 4

3.1 Synthesis of **AQ** ..... 4

3.2 Synthesis of **$PMo_{10}V_2$** ..... 6

3.3 Synthesis of **$PW_{10}V_2$** ..... 6

3.4 Synthesis of **POMOF 1** ..... 7

3.5 Synthesis of **POMOF 2** ..... 7

3.6 Synthesis of **POMOF 3** ..... 8

4. Crystallographic data and crystal structures of **POMOF 1-3** ..... 10

5. Additional Characterizational Figures of **POMOF 1-3** ..... 15

5.1 PXRD spectra of **POMOF 2-3** ..... 15

5.2 TGA curve of **POMOF 2-3** ..... 16

5.3 FT-IR spectra of **POMOF 1-3** ..... 17

5.4 Stability test of **POMOF 1** ..... 18

5.5 Dye adsorption by **POMOF 1-3** ..... 19

5.6 XPS survey spectra of **POMOF 1-3** ..... 20

5.7 Estimated energy band gaps of **POMOF 1-3** ..... 23

5.8 Mott−Schottky plots of **POMOF 1-3** ..... 25

6. General procedures for Photocatalytic Oxidation of Benzylamines ..... 27

7. $^1$H NMR spectrum of photocatalytic oxidation products ..... 34

8. References ..... 39

## 1. Materials

All chemicals were purchased commercially and used without further purification.

## 2. Instrumentation

**Crystallography:** Suitable single crystals were selected and mounted onto a rubber loop using Fomblin oil. Single crystal X-ray diffraction data of **POMOF 1 - POMOF 3** were recorded on a Bruker/ARINAX MD2 diffractometer equipped with a MarCCD-300 detector at beam line station BL17B of Shanghai Synchrotron Radiation Facility (SSRF) at 150 K. The structures were solved by the direct methods and refined with OLEX 2-1.5. All non-hydrogen atoms are anisotropic refined by the least square method, and the hydrogen atoms are determined by the ideal geometry by the theoretical hydrogenation method. CCDC-2431828 (**POMOF 1**), CCDC-2431829 (**POMOF 2**), CCDC-2431830 (**POMOF 3**) contain the supplementary crystallographic data for this paper. These data can be obtained free of charge via www.ccdc.cam.ac.uk/data_request/cif.

**Element Analyses:** Element analyses C, N and H content were determined by VARIDEL III Elemental Analyzer.

**Thermogravimetric Analysis (TGA):** Thermogravimetric analysis was performed on a METTLER TOLEDO TG8000 Thermogravimetric Analyzer under nitrogen flow at a typical heating rate of 10 °C·min$^{-1}$.

**Powder X-ray Diffraction (PXRD):** Powder XRD was recorded on a Haoyuan DX-2700B diffractometer equipped with monochromatized Cu-Kα (λ = 1.5418 Å) radiation in the range of 3° ≤ 2θ ≤ 50º, with a scanning rate of 0.02° s$^{-1}$.

**Fourier-transform infrared (FT-IR) spectroscopy:** The samples were prepared as a KBr pellet and the FT-IR spectrum was collected in transmission mode in the range of 600-4000 cm$^{-1}$ using a NEXUS-670 spectrometer. Wavenumbers are given in cm$^{-1}$. Intensities are denoted as w = weak, m = medium, s = strong, vs = very strong, br = broad.

**Solid-state UV-Vis absorption spectroscopy:** All compounds were prepared into powders, which were tested in wavelength mode by integrating sphere attachment in UV3600 UV-Vis spectrometer.

**Mott-Schottky**: Mott-Schottky plot was conducted on an electrochemical workstation CHI 760D. Firstly, the lapping sample (5 mg) was dispersed in ethanol (1 mL), and Nafion (100 μL) was added to the sample for ultrasonic mixing. Appropriate suspension droplets were taken on the fluoride-tin oxide (FTO) glass plate (1 × 2 $cm^2$, 50 Ω/$cm^2$) as the working electrode, Pt wire as the counter electrode. Ag/AgCl was used as the reference electrode and 0.5 mol/L $Na_2SO_4$ solution was used as the electrolyte. Under a certain pressure range, frequencies of 1000 Hz, 1500 Hz and 2000 Hz were selected for testing.

## 3. Synthesis

### 3.1 Synthesis of AQ

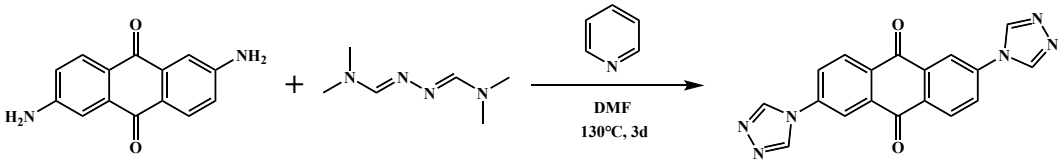


**Figure S1.** The synthesis procedure of **AQ**.

2,6-di (4H-1,2,4-triazol-4-yl) anthracene-9,10-dione (**AQ)** was synthesized according to the literature.[1] A mixture of 1.4 g 2,6-Diaminoanthraquinone (5.9 mmol), 5.2 g N,N-dimethylformamide azine (36.5 mmol) in DMF (20 mL) and pyridine (25 mL) was heated at 130 ℃ for 72 h. The reaction mixture was cooled to room temperature and the brown precipitate was collected by filtration and washed with $CH_3CN$. Yield: 1.1 g (55%).

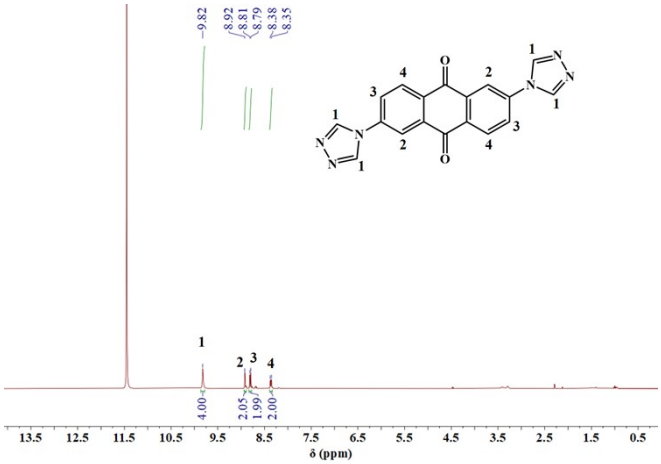


**Figure S2.** The $^1H$ NMR (400 MHz, $CF_3COOD$, ppm) spectrum of **AQ**.

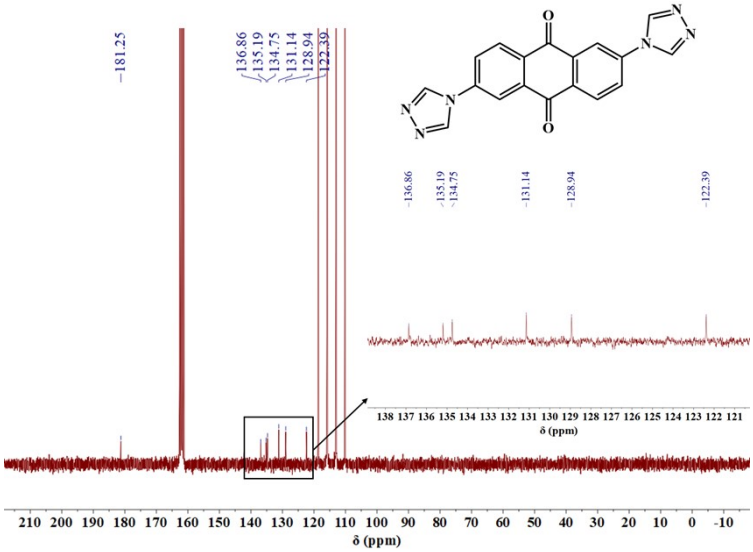


**Figure S3.** The $^{13}C$ NMR (400 MHz, $CF_3COOD$, ppm) spectrum of **AQ**.

### 3.2 Synthesis of $PMo_{10}V_2$

The synthesis of $H_5[PMo_{10}V_2O_{40}] \cdot 32H_2O$ ($PMo_{10}V_2$) is based on the previously reported literature.[2] The specific synthesis process is as follows: The $NaVO_3$ (30.0 g), 85% $H_3PO_4$ (3.4 mL), and $MoO_3$ (74.0 g) were added to 800 mL of water and refluxed for 8 h. Afterwards, the mixture was acidified using 145 mL of 12M HCl, and the resulting acid was extracted with 200 mL of diethyl ether. Finally, the diethyl ether was removed, and the product was obtained by recrystallization from water. ICP (%) calcd for $PMo_{10}V_2O_{72}H_{69}$: Mo 41.46, V 4.40; found: Mo 41.89, V 4.48.

**Table S1.** ICP Analysis of $PMo_{10}V_2$.

| Element | Mo | V |
|---|---|---|
| Calculated value (%) | 41.46 | 4.40 |
| Actual value (%) | 41.89 | 4.48 |

### 3.3 Synthesis of $PW_{10}V_2$

$H_5[PW_{10}V_2O_{40}] \cdot 30H_2O$ ($PW_{10}V_2$) was synthesized according to the method previously reported in

the literature.[3] Typically, sodium metavanadate ($NaVO_3$, 12.2 g, 100 mmol) was dissolved in 50 mL of boiling water and mixed with disodium hydrogen phosphate ($Na_2HPO_4$, 3.55 g, 25 mmol), already dissolved in 50 mL of water. After the resulting solution was cooled to room temperature, concentrated sulfuric acid (5 mL, 17 mol/L, 85 mmol) was added to the mixture to give a red solution. Sodium tungstate dihydrate ($Na_2WO_4{\cdot}2H_2O$, 82.5 g, 250 mmol) was dissolved in 100 mL of water and added to the red solution with vigorous stirring, followed by the slow addition of concentrated sulfuric acid (42 mL, 17 mol/L, 714 mmol). Extraction of the solution with diethyl ether (500 mL), followed by evaporation in air, produced $PW_{10}V_2$ as a crystalline, orange-red solid (yield, 74 %). ICP (%) calcd for $PW_{10}V_2O_{70}H_{65}$: W 58.24, V 3.23; found: W 60.07, V 3.41.

**Table S2.** ICP Analysis of $PW_{10}V_2$.

| Element | W | V |
|---|---|---|
| Calculated value (%) | 58.24 | 3.23 |
| Actual value (%) | 60.07 | 3.41 |

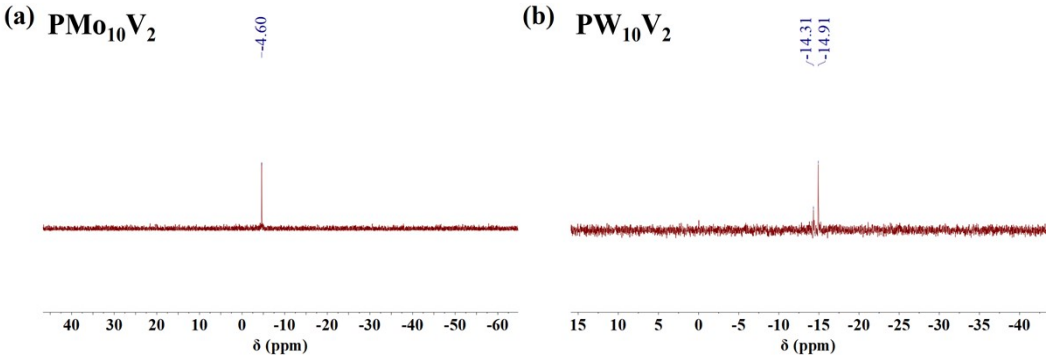


**Figure S4.** $^{31}$P-NMR spectra of (a) $PMo_{10}V_2$ and (b) $PW_{10}V_2$.

### 3.4 Synthesis of POMOF 1

$H_3[Cd_2Br(H_2O)_4(CH_3CN)(C_{18}H_{10}N_6O_2)_2(PMo_{10}V_2O_{40})]{\cdot}7H_2O$ (**POMOF 1**) was synthesized by self-assembly method under hydrothermal conditions. $H_5[PMo_{10}V_2O_{40}]$ ·$32H_2O$ (22.8 mg, 0.01 mmol), $CdBr_2{\cdot}4H_2O$ (13.8 mg, 0.04 mmol), **AQ** (6.8 mg, 0.02 mmol) were dissolved in a mixed solution of water and acetonitrile ($V_1$ / $V_2$ =1:3). After stirring at 800 r / min for 1 h, the mixture is transferred to a 10 mL bottle containing a high temperature resistant plastic lid and a rubber inner

plug, and then heated in an oven at 120 °C for 24 h. The orange long crystals were collected by filtration, washed with acetonitrile, and dried in an air atmosphere (based on $H_5[PMo_{10}V_2O_{40}]$ $\cdot 32H_2O$, yield 51 %). EA and ICP (%) calcd for $C_{38}H_{48}BrCd_2Mo_{10}N_{13}O_{55}PV_2$: Cd 7.58, Mo 32.37, V 3.43, C 15.40, H 1.63, N 6.14, P 1.04, Br 2.70; found: Cd 8.05, Mo 33.89, V 3.61, C 16.45, H 1.66, N 6.51, P 1.08, Br 2.61.

**3.5 Synthesis of POMOF 2**

$H_3[Cd_2I(H_2O)_4(CH_3CN)(C_{18}H_{10}N_6O_2)_2(PMo_{10}V_2O_{40})]\cdot 12H_2O$ (**POMOF 2**) was synthesized by self-assembly method under hydrothermal conditions. $H_5[PMo_{10}V_2O_{40}]$ $\cdot 32H_2O$ (22.8 mg, 0.01 mmol), $CdI_2$ (14.6 mg, 0.04 mmol), **AQ** (6.8 mg, 0.02 mmol) were dissolved in a mixed solution of water and acetonitrile ($V_1$ / $V_2$ = 1:3). After stirring at 800 r / min for 1 h, the mixture is transferred to a 10 mL bottle containing a high temperature resistant plastic lid and a rubber inner plug, and then heated in an oven at 120 °C for 24 h. Yellow needle-like crystals were collected by filtration, washed with acetonitrile, and dried in an air atmosphere (based on $H_5[PMo_{10}V_2O_{40}]$ $\cdot 32H_2O$, yield 43 %). EA and ICP (%) calcd for $C_{38}H_{58}Cd_2IMo_{10}N_{13}O_{60}PV_2$: Cd 7.25, Mo 30.94, V 3.29, C 14.72, H 1.88, N 5.87, P 1.00, I 4.09; found: Cd 7.83, Mo 32.45, V 3.60, C 14.07, H 1.65, N 5.32, P 1.06, I 4.38.

**3.6 Synthesis of POMOF 3**

$H_3[Cd_2Br(H_2O)_4(CH_3CN)(C_{18}H_{10}N_6O_2)_2(PW_{10}V_2O_{40})]\cdot 14H_2O$ (**POMOF 3**) was synthesized by self-assembly method under hydrothermal conditions. $H_5[PW_{10}V_2O_{40}]$ $\cdot 30H_2O$ (12.5 mg, 0.004 mmol), $CdBr_2\cdot 4H_2O$ (13.8 mg, 0.04 mmol), **AQ** (6.8 mg, 0.02 mmol) were dissolved in a mixed solution of water and acetonitrile ($V_1$ / $V_2$ = 1:3). After stirring at 800 r / min for 1 h, the mixture is transferred to a 10 mL bottle containing a high temperature resistant plastic lid and a rubber inner plug, and then heated in an oven at 120 °C for 36 h. The orange long crystals were collected by filtration, washed with acetonitrile, and dried in an air atmosphere (based on $H_5[PW_{10}V_2O_{40}]$ $\cdot 30H_2O$, yield 31 %). EA and ICP (%) calcd for $C_{38}H_{62}BrCd_2N_{13}O_{62}PV_2W_{10}$: Cd 5.66, W 46.32, V 2.57, C 11.49, H 1.57, N 4.58, P 0.78, Br 2.01; found: Cd 6.14, W 48.96, V 2.76, C 11.56, H 1.46, N 4.27, P 0.76, Br 2.21.

**Table S3.** ICP Analysis of Mo、W and V in **POMOF 1−POMOF 3**.

| | | Calculated value (%) | Actual value (%) | | |
|---|---|---|---|---|---|
| | | | 1st Test | 2nd Test | 3rd Test |
| **POMOF 1** | Mo | 32.37 | 33.89 | 33.97 | 34.15 |
| | V | 3.43 | 3.61 | 3.67 | 3.74 |
| **POMOF 2** | Mo | 30.94 | 32.45 | 32.57 | 29.11 |
| | V | 3.29 | 3.60 | 3.41 | 3.39 |
| **POMOF 3** | W | 46.32 | 48.96 | 49.11 | 49.02 |
| | V | 2.57 | 2.76 | 2.78 | 2.85 |

4. Crystallographic data and crystal structures of POMOF 1-3

**Table S4.** Crystal data and structure refinement for **POMOF 1**

| Compound | **POMOF 1** |
|---|---|
| Empirical formula | $BrC_{38.27}Cd_2H_{58.86}Mo_{10}N_{13.14}O_{61.73}PV_2$ |
| Formula weight | 3087.62 |
| Crystal system | monoclinic |
| Space group | *I*2/a |
| a /Å | 15.2326(11) Å |
| b /Å | 21.4831(18) Å |
| c /Å | 25.4527(18) Å |
| α/° | 90° |
| β/° | 97.523(4)° |
| γ/° | 90° |
| V /Å$^3$ | 8257.5(11) Å$^3$ |
| Z | 4 |
| ρ calc /g·cm$^{-3}$ | 2.484 Mg/m$^3$ |
| μ(MoKα) /mm$^{-1}$ | 2.562 mm$^{-1}$ |
| F(000) | 5945.0 |
| 2θ range /° | 2.412 to 49.046° |
| Index ranges | -18<=h<=17, -25<=k<=25, -30<=l<=30 |
| Reflections collected | 91825 |
| Data / restraints / parameters | 7476 / 1061 / 777 |
| $R_1/wR_2$ (I>2σ(I))[a] | $R_1$ = 0.0362, $wR_2$ = 0.0918 |
| $R_1/wR_2$ (all data) | $R_1$ = 0.0369, $wR_2$ = 0.0922 |
| GooF (all data)[b] | 1.132 |
| Data completeness | 98.8 % |

[a] $R_1 = \sum||Fo|-|Fc||/\sum|Fo|$; $wR_2 = \{\sum w[(Fo)^2-(Fc)^2]^2/\sum w[(Fo)^2]^2\}^{1/2}$

[b] $GooF = \{\sum w[(Fo)^2-(Fc)^2]^2/(n-p)\}^{1/2}$

**Table S5.** Crystal data and structure refinement for **POMOF 2**

| Compound | **POMOF 2** |
|---|---|
| Empirical formula | $C_{38.89}Cd_2Cl_{0.28}H_{60.95}I_{0.72}Mo_{10}N_{13.45}O_{62.31}PV_2$ |
| Formula weight | 3132.46 |
| Crystal system | monoclinic |
| Space group | *I*2/a |
| a /Å | 15.2182(12) Å |
| b /Å | 21.5762(14) Å |
| c /Å | 25.4191(18) Å |
| α/° | 90° |
| β/° | 97.534(4)° |
| γ/° | 90° |
| V /Å$^3$ | 8274.3(10) Å$^3$ |
| Z | 4 |
| ρ calc /g·cm$^{-3}$ | 2.515 Mg/m$^3$ |
| μ(MoKα) /mm$^{-1}$ | 2.597 mm$^{-1}$ |
| F(000) | 6028.0 |
| 2θ range /° | 3.232 to 50.76° |
| Index ranges | -18<=h<=18, -25<=k<=25, -30<=l<=30 |
| Reflections collected | 97999 |
| Data / restraints / parameters | 7560 / 1127 / 789 |
| $R_1$/w$R_2$ (I>2σ(I))[a] | $R_1$ = 0.0381, w$R_2$ = 0.0912 |
| $R_1$/w$R_2$ (all data) | $R_1$ = 0.0388, w$R_2$ = 0.0917 |
| GooF (all data)[b] | 1.116 |
| Data completeness | 99.6 % |

[a] $R_1 = \sum||Fo|-|Fc||/\sum|Fo|$; $wR_2 = \{\sum w[(Fo)^2-(Fc)^2]^2/\sum w[(Fo)^2]^2\}^{1/2}$

[b] $GooF = \{\sum w[(Fo)^2-(Fc)^2]^2/(n-p)\}^{1/2}$

**Table S6.** Crystal data and structure refinement for **POMOF 3**

| Compound | **POMOF 3** |
|---|---|
| Empirical formula | $BrC_{38.02}Cd_2H_{76.99}N_{13.01}O_{70.98}PV_2W_{10}$ |
| Formula weight | 4128.22 |
| Crystal system | monoclinic |
| Space group | *I*2/a |
| a /Å | 15.2114(15) Å |
| b /Å | 21.527(2) Å |
| c /Å | 25.359(3) Å |
| α/° | 90° |
| β/° | 97.727(6)° |
| γ/° | 90° |
| V /Å$^3$ | 8228.6(15) Å$^3$ |
| Z | 4 |
| ρ calc /g·cm$^{-3}$ | 3.332 Mg/m$^3$ |
| μ(MoKα) /mm$^{-1}$ | 13.992 mm$^{-1}$ |
| F(000) | 7584.0 |
| 2θ range /° | 3.142 to 49.234° |
| Index ranges | -18<=h<=18, -25<=k<=25, -30<=l<=30 |
| Reflections collected | 69912 |
| Data / restraints / parameters | 7555 / 1031 / 789 |
| $R_1/wR_2$ (I>2σ(I))[a] | $R_1$ = 0.0545, $wR_2$ = 0.1476 |
| $R_1/wR_2$ (all data) | $R_1$ = 0.0560, $wR_2$ = 0.1486 |
| GooF (all data)[b] | 1.062 |
| Data completeness | 99.6 % |

[a] $R_1 = \sum||Fo|-|Fc||/\sum|Fo|$; $wR_2 = \{\sum w[(Fo)^2-(Fc)^2]^2/\sum w[(Fo)^2]^2\}^{1/2}$

[b] $GooF = \{\sum w[(Fo)^2-(Fc)^2]^2/(n-p)\}^{1/2}$

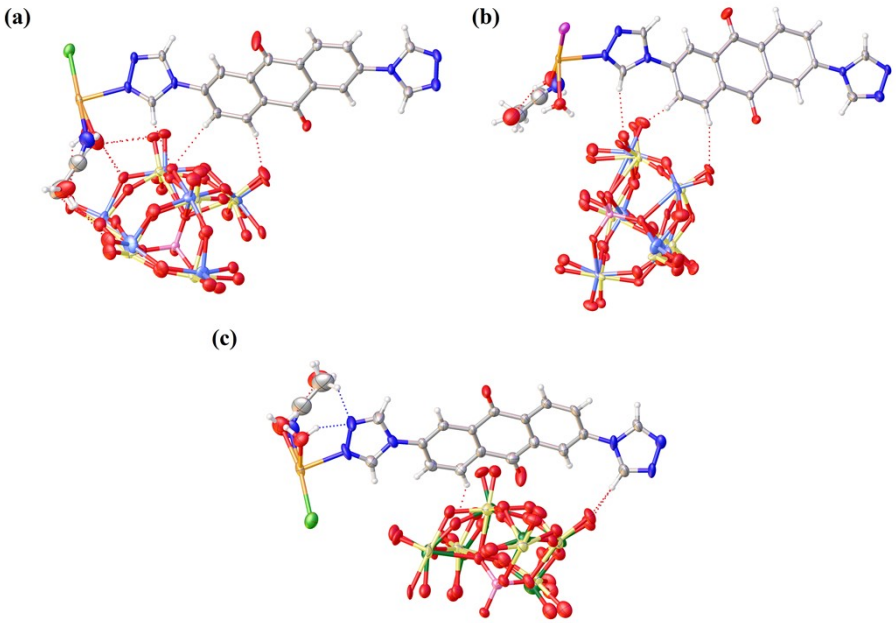


**Figure S5.** (a) Asymmetric unit of **POMOF 1**, (b) asymmetric unit of **POMOF 2**, (c) asymmetric unit of **POMOF 3**. All the atoms are presented in thermal ellipsoids with a 50% probability level (Color Code: Cd, orange; C, grey; N, deep blue; Br, green; I, purple; O, red; Mo, blue; W, dark green; V, yellow; P, pink; H, white.)

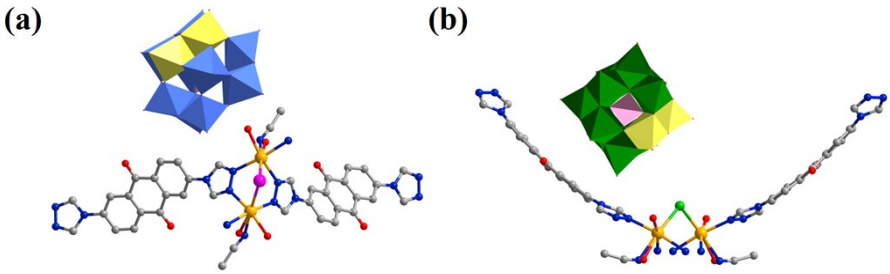


**Figure S6.** (a)The structural unit diagram of **POMOF 2**, (b)the structural unit diagram of **POMOF 3**. (Color Code: Cd, orange; C, grey; N, deep blue; Br, green; I, purple; O, red; Mo, blue; W, dark green; V, yellow; P, pink. H Atoms are omitted for clarity.)

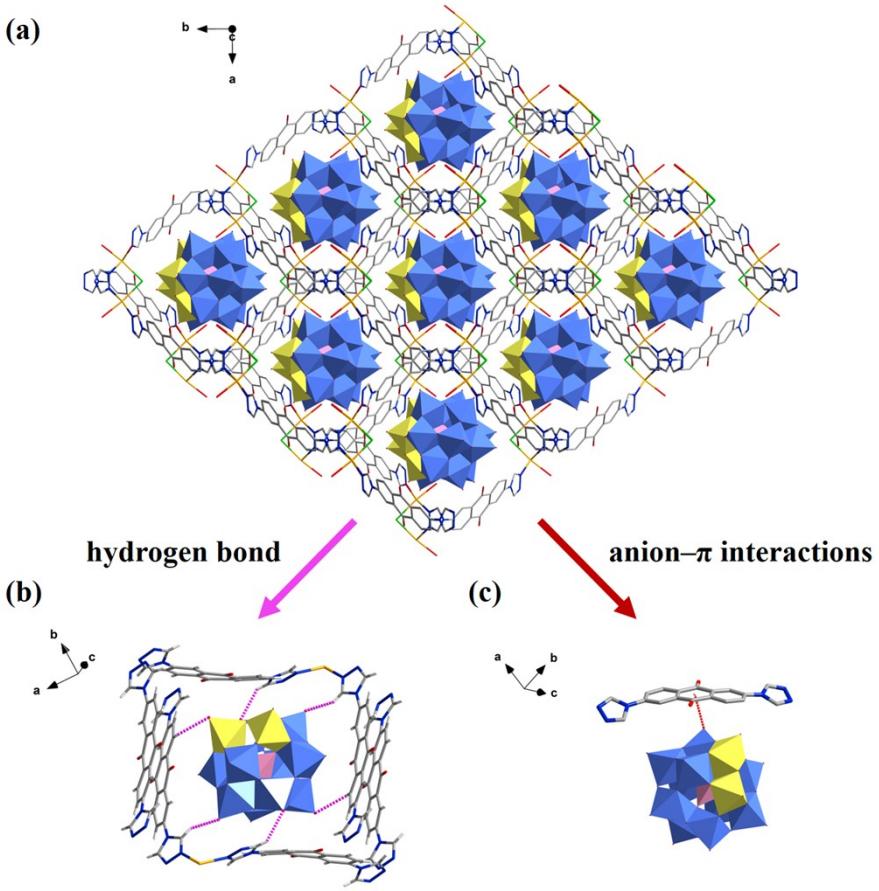


**Figure S7.** (a) The stacking diagram of **POMOF 1** along the *c*-axis direction, (b) the hydrogen bonding interaction between one $PMo_{10}V_2$ and four **AQ** ligands in **POMOF 1**, (c) the anion–π interactions between the adjacent $PMo_{10}V_2$ and **AQ** in **POMOF 1**. (Color Code: Cd, orange; C, grey; N, deep blue; Br, green; I, purple; O, red; Mo, blue; W, dark green; V, yellow; P, pink; H, white.)

## 5. Additional Characterizational Figures of POMOF 1-3

### 5.1 PXRD spectra of POMOF 2-3

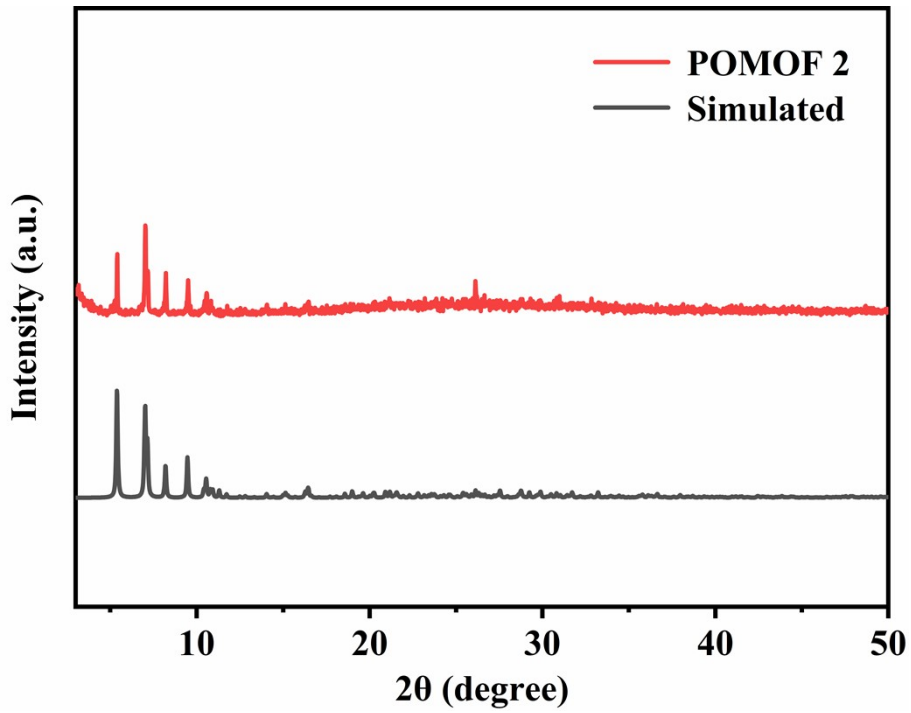


**Figure S8.** Experimental and simulated PXRD patterns of **POMOF 2**.

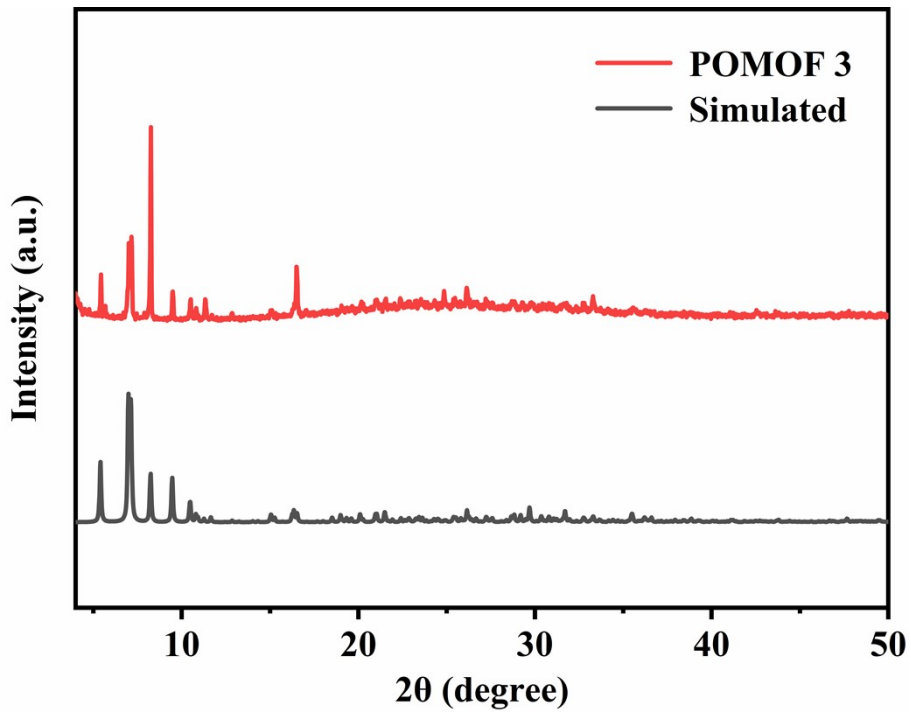


**Figure S9.** Experimental and simulated PXRD patterns of **POMOF 3**.

**5.2 TGA curve of POMOF 2-3**

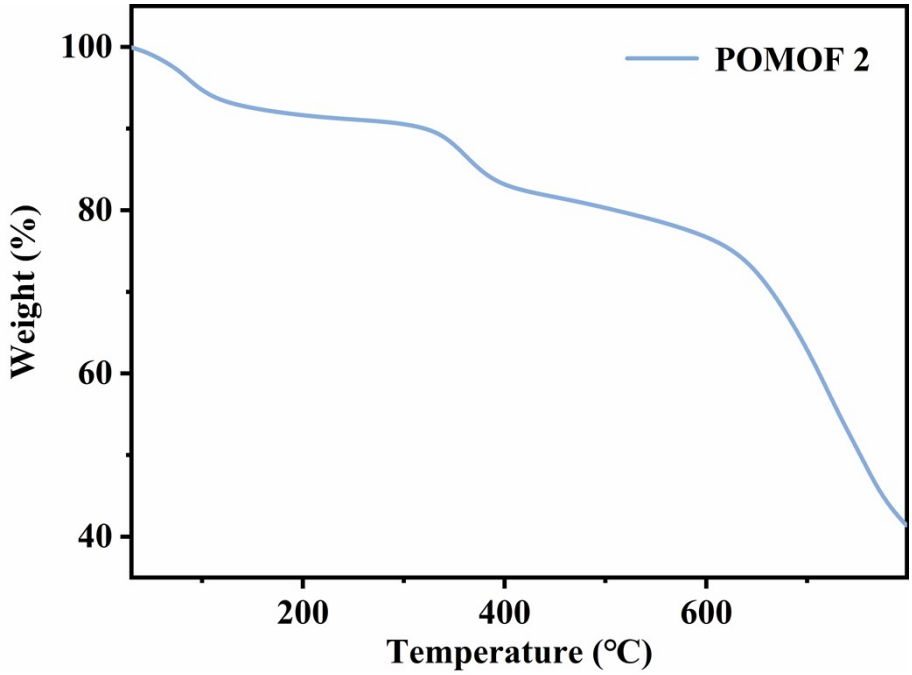


**Figure S10.** TGA curve of **POMOF 2**.

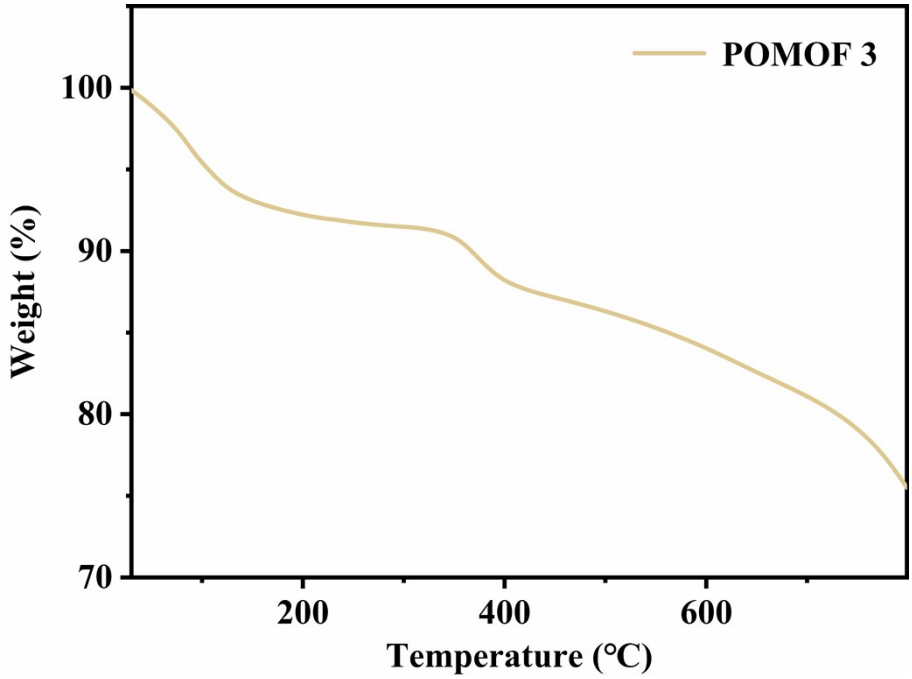


**Figure S11.** TGA curve of **POMOF 3**.

**5.3 FT-IR spectra of POMOF 1-3**

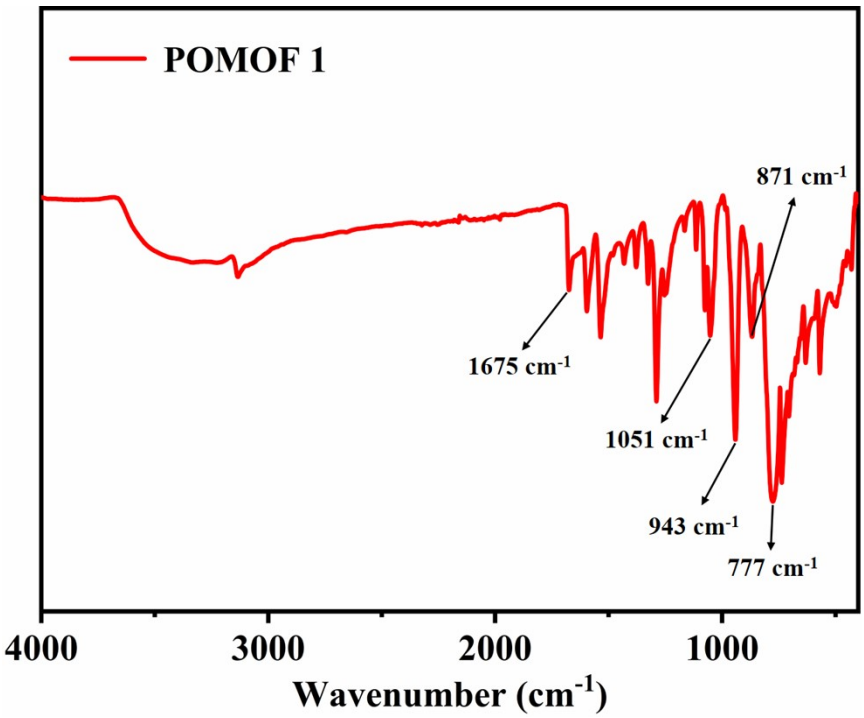


**Figure S12.** FT-IR spectrum of **POMOF 1**.

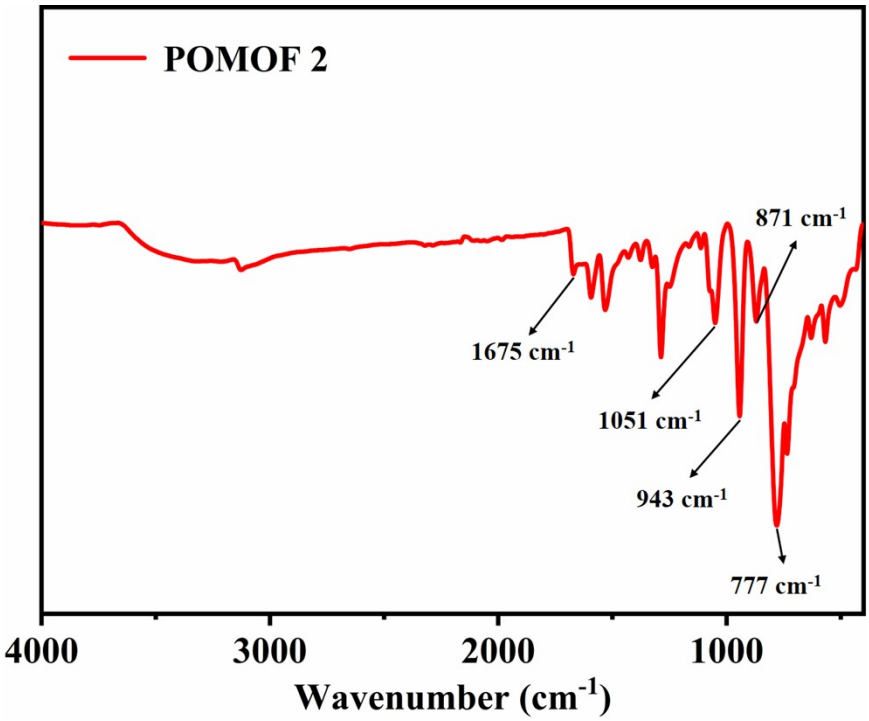


**Figure S13.** FT-IR spectrum of **POMOF 2**.

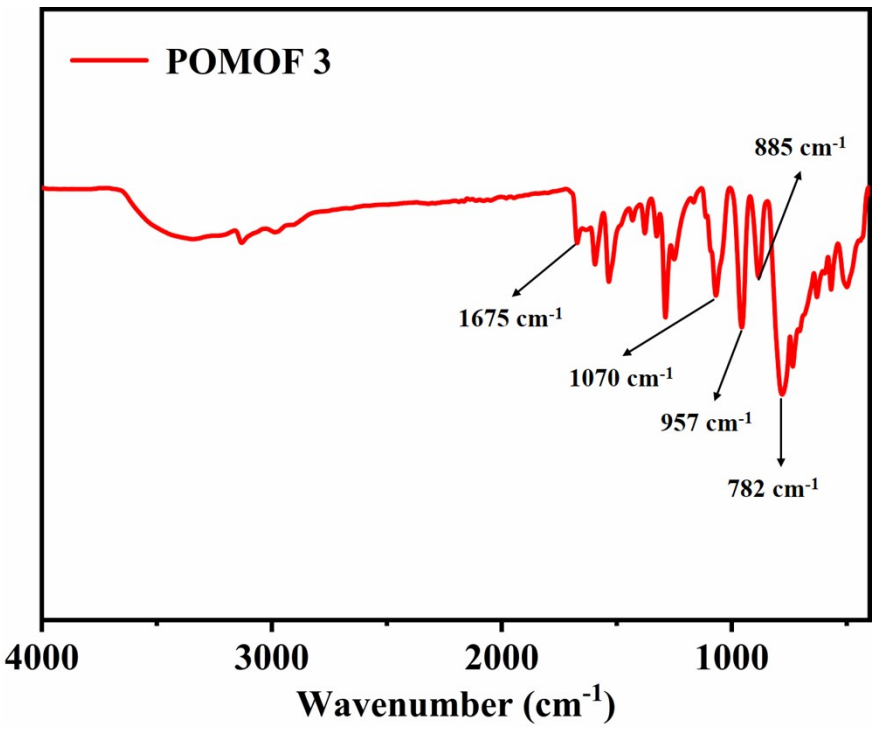


**Figure S14.** FT-IR spectrum of **POMOF 3**.

### 5.4 Stability test of POMOF 1

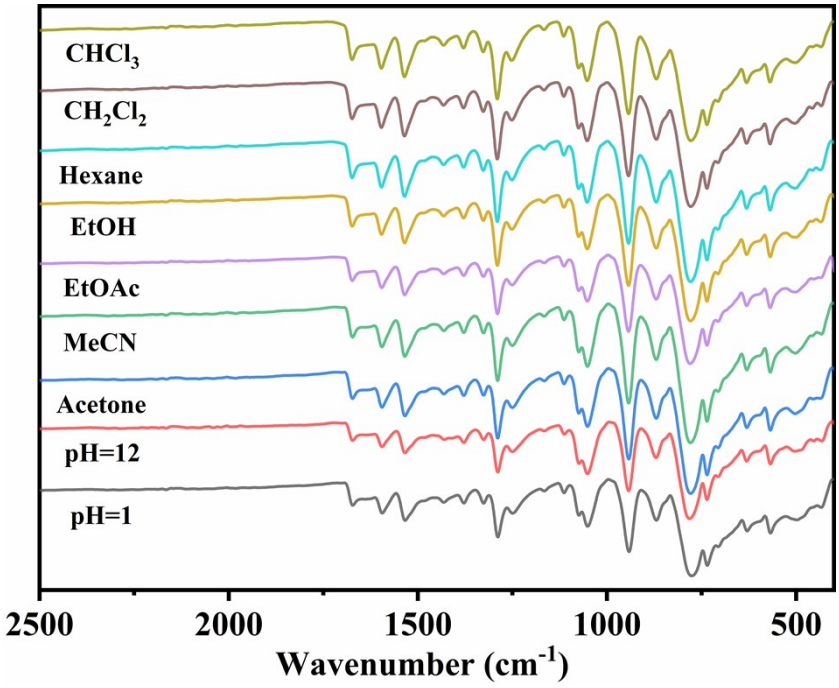


**Figure S15.** FT-IR spectra of **POMOF 1** after soaked in different organic solvents and pH for 24 hours.

**5.5 Dye adsorption by POMOF 1-3**

Preparation of the working curves of Dyes: The standard solutions of 4-[4-dimethylamino]styryl)-1-methylpyridinium (DASP) was prepared in a sequential concentration of 1mg/L, 5mg/L, 10mg/L, 15mg/L and 20mg/L, respectively. These standard solutions were then tested by Uv-Vis spectrometer to make working curves based on the relationship between absorption and concentration.

Dye adsorption experiment: Taking 3 mL of 30mg/L standard solution (DASP) into a 10 mL glass bottle, 3 mg **POMOF 1**/**POMOF 2**/**POMOF 3** was subsequently added and stirred for 6 hours. The solution was then filtered and used for testing its absorbance with a spectrometer. The amount of absorbed dye molecules per formula was evaluated by comparing their absorbances with the working curves.

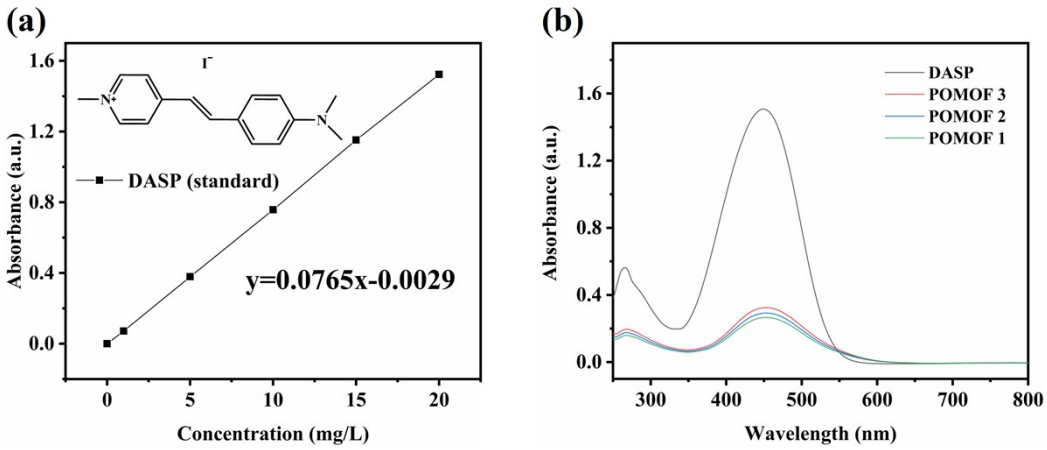


**Figure S16.** UV-Vis absorption spectra of DASP solution before and after adsorption by **POMOF 1-3**. DASP (30 mg/L, 3 mL), POMOF (3 mg), 6 h.

**5.6 XPS survey spectra of POMOF 1-3**

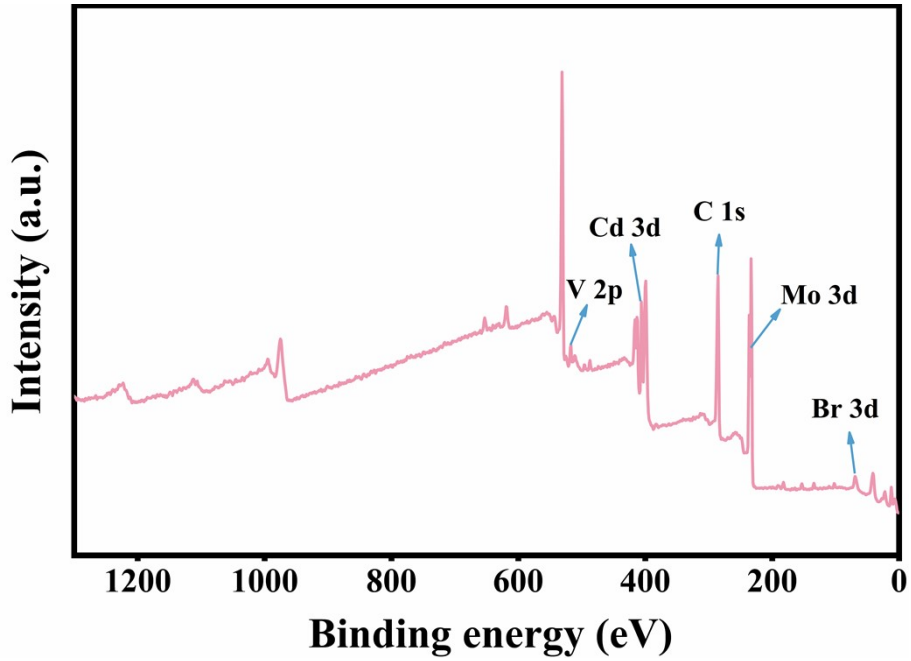


**Figure S17.** XPS survey spectra of **POMOF 1**.

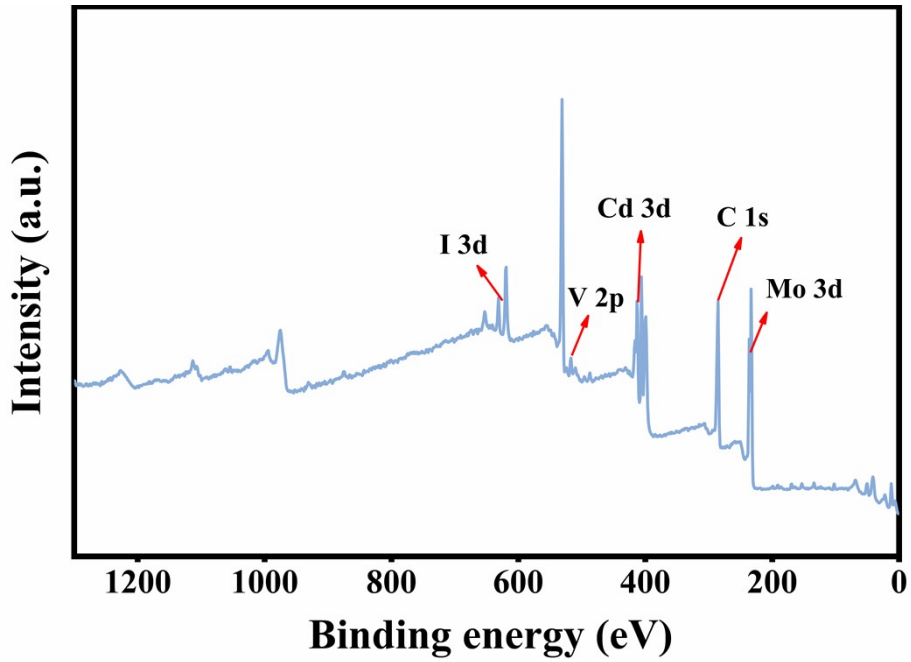


**Figure S18.** XPS survey spectra of **POMOF 2**.

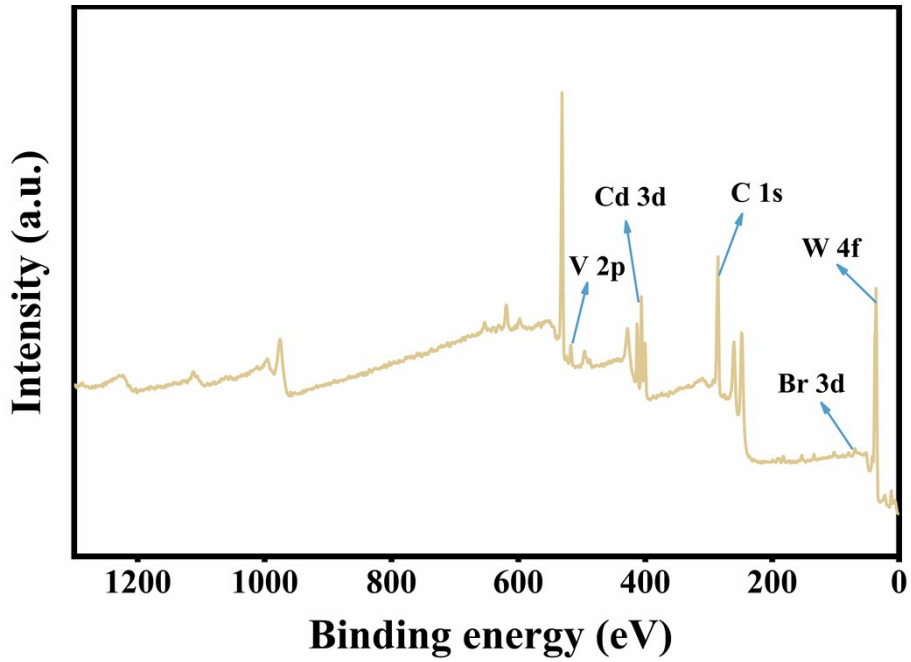


**Figure S19.** XPS survey spectra of **POMOF 3**.

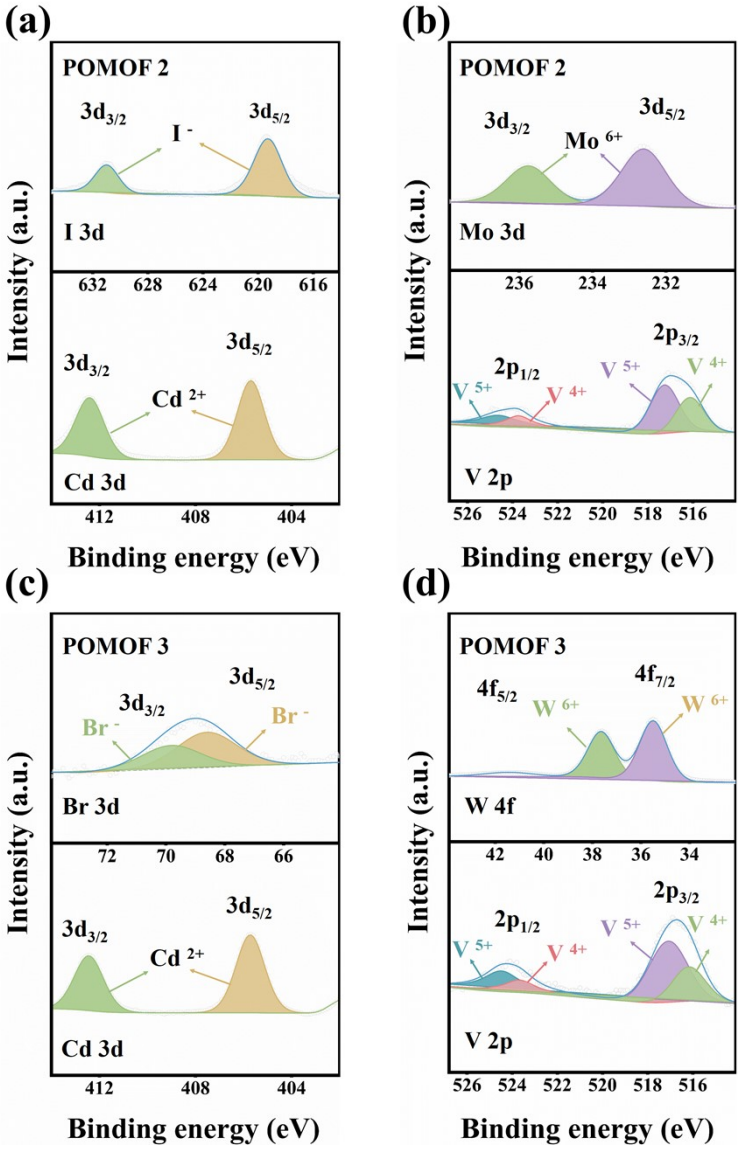


**Figure S20.** (a-b) Resolved I 3d, Cd 3d, Mo 3d, V 2p, XPS core-level spectra of **POMOF 2**, (c-d) Resolved Br 3d, Cd 3d, W 4f, V 2p, XPS core-level spectra of **POMOF 3**.

**5.7 Estimated energy band gaps of POMOF 1-3**

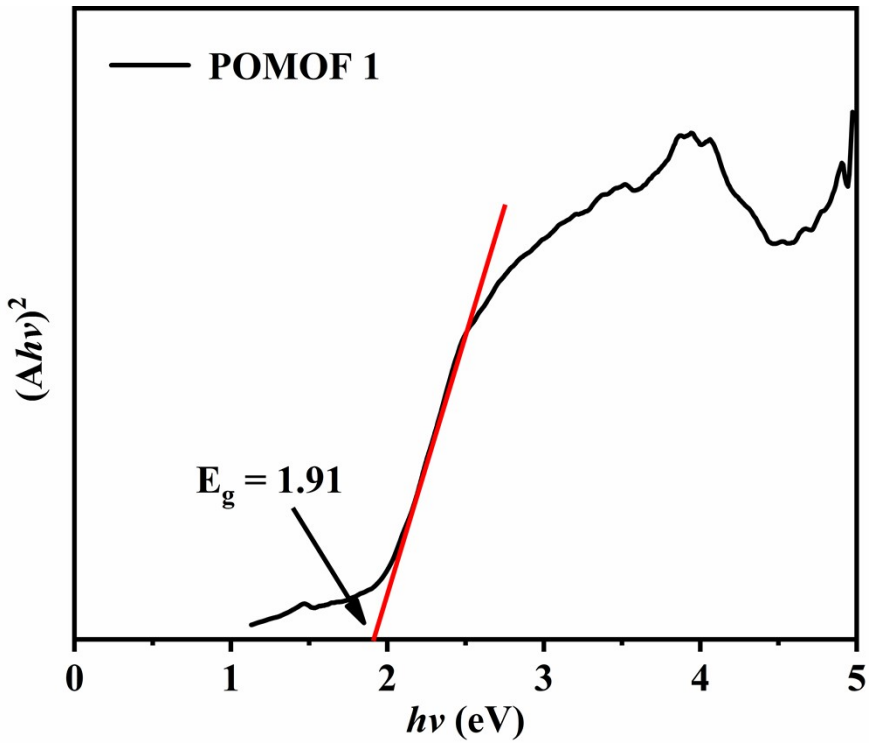


**Figure S21.** Tauc plots of **POMOF 1**.

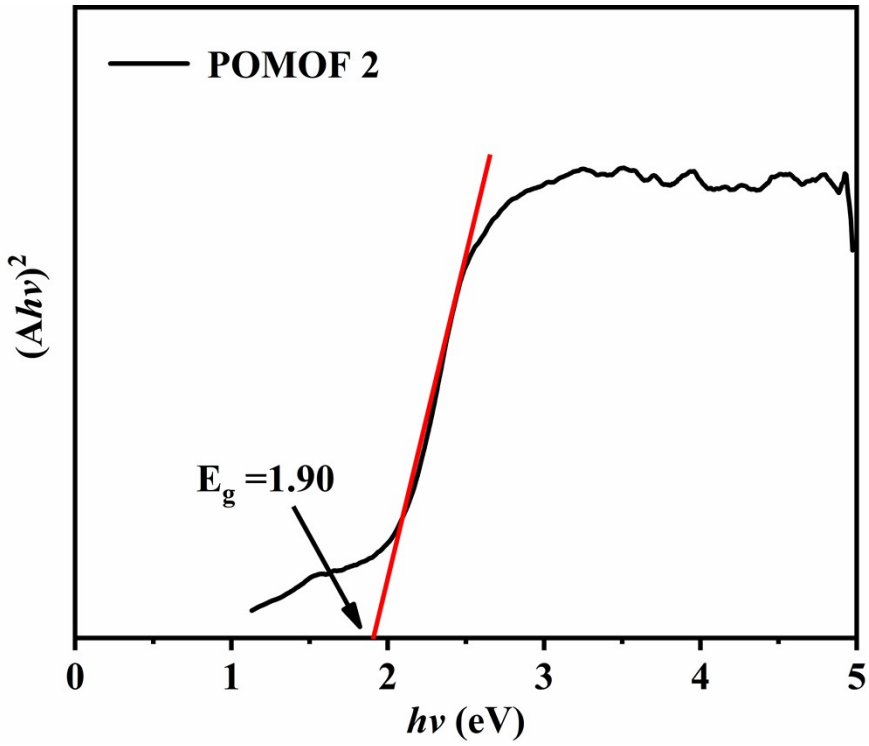


**Figure S22.** Tauc plots of **POMOF 2**.

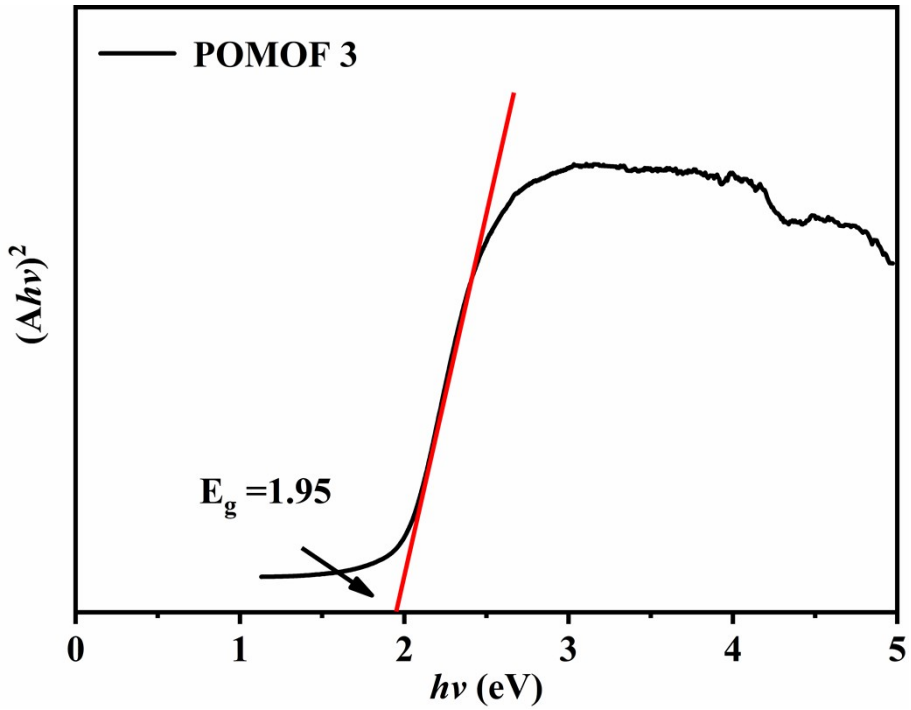


**Figure S23.** Tauc plots of **POMOF 3**.

**5.8 Mott−Schottky plots of POMOF 1-3**

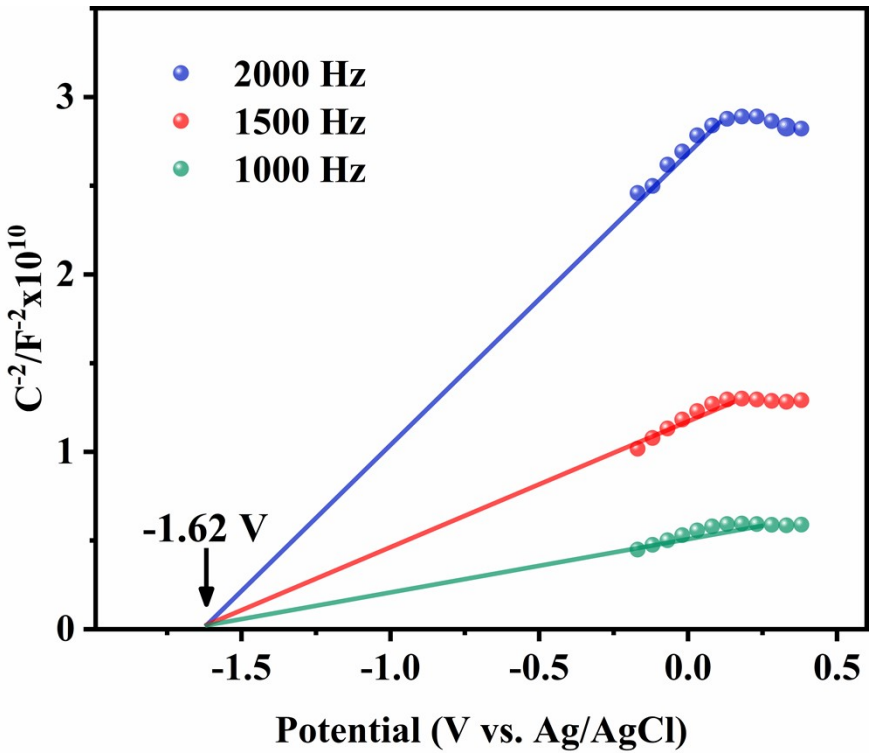


**Figure S24.** Mott−Schottky plots of **POMOF 1**.

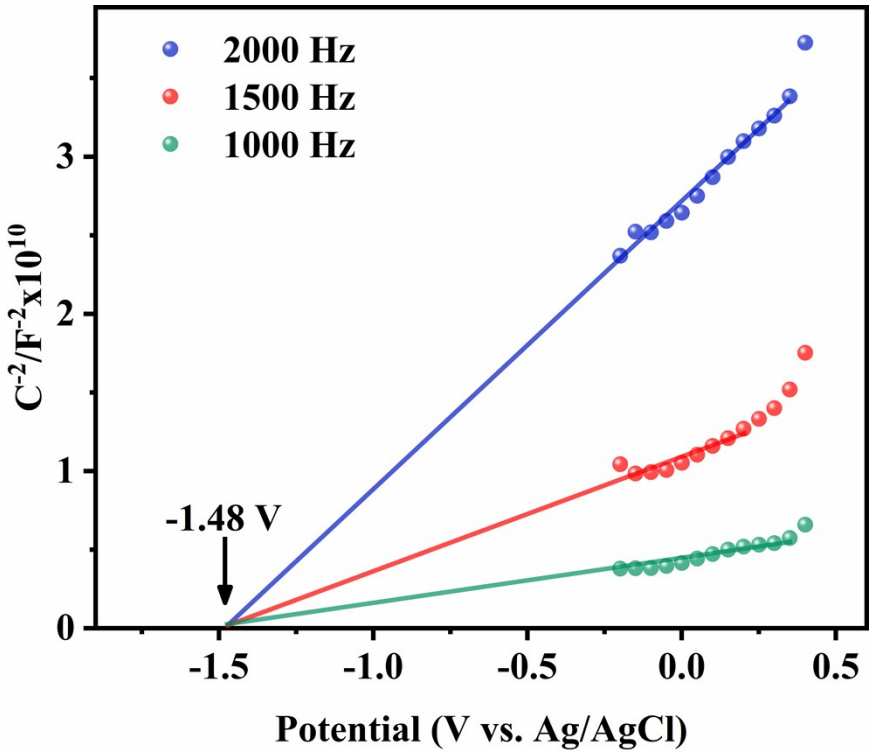


**Figure S25.** Mott−Schottky plots of **POMOF 2**.

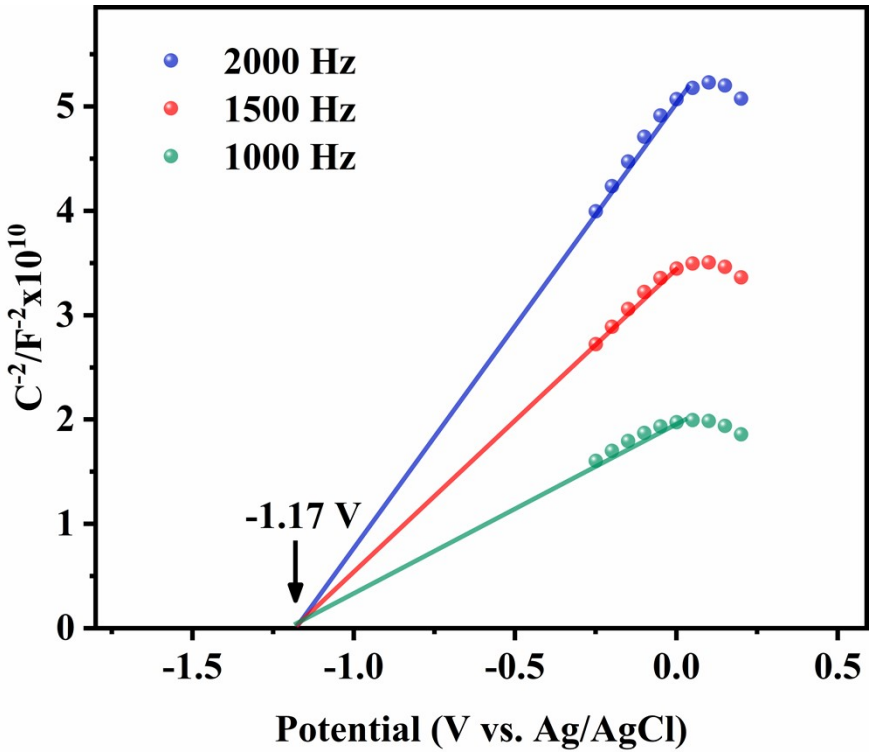


**Figure S26.** Mott−Schottky plots of **POMOF 3**.

## 6. General procedures for Photocatalytic Oxidation of Benzylamines

All manipulations were conducted under aerobic condition. Into a test tube (φ 20 mm × 170 mm) equipped with an $O_2$ balloon (1 atm) were successively placed catalyst, benzylamine (0.1 mmol) and $CH_3CN$ (1 mL). A Teflon-coated magnetic stir bar was added, and the mixture was irradiated with poper light sources with stirring at room temperature for 24 h. When performing quenching experiments, 0.4 eq. scavenger was added to the above reactants. The products were confirmed using GC and GC-Mass, and the conversion was calculated with respect to the internal standard (N-hexadecane). After the reaction, the catalysts was recovered by centrifugation, washed with $CH_3CN$, and then air-dried prior to being used for the cycle experiment.

**Figure S27.** Image of photocatalytic device.

**Table S7.** Visible-light-driven photocatalytic oxidative coupling of benzylamine. [a]

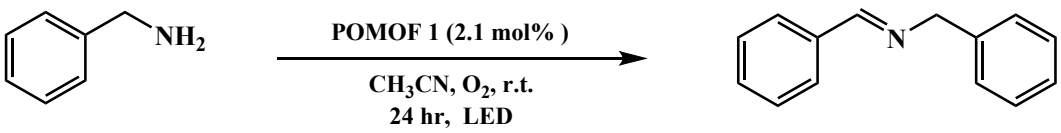


| Entry | Light sources | Yield (%)[b] |
|---|---|---|
| 1 | 500 nm | 98 |
| 2 | 585 nm | 17 |
| 3 | 660 nm | 8 |

[a]Reaction conditions: reactant (0.10 mmol), **POMOF 1** (2.1 mol%), $CH_3CN$ (1.0 mL), r.t., 24 h,

LED (10 W), $O_2$. The yield rate was determined by [b]GC. (N-hexadecane was used as the internal standard substance, Sel.: 99%)

**Table S8.** Screening the catalyst dosage for Photocatalytic Oxidation of Benzylamines. [a]

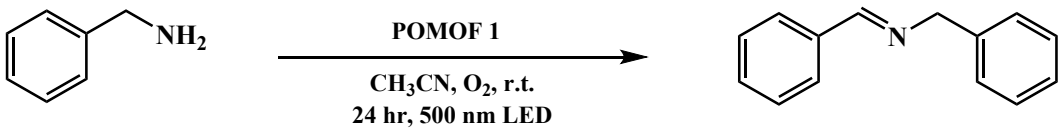


| Entry | Catalyst dosage | Yield (%)[b] |
|---|---|---|
| 1 | 1.4 mol% | 74 |
| 2 | 2.1 mol% | 98 |
| 3 | 2.8 mol% | 87 |

[a]Reaction conditions: reactant (0.10 mmol), **POMOF 1** (x mol%), $CH_3CN$ (1.0 mL), r.t., 24 h, LED (10 W), $O_2$. The yield rate was determined by [b]GC. (N-hexadecane was used as the internal standard substance, Sel.: 99%)

**Table S9.** Screening the solvents for Photocatalytic Oxidation of Benzylamines. [a]

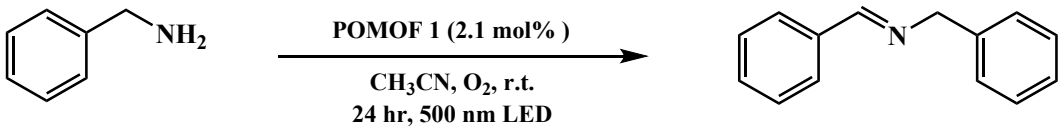


| Entry | Solvent | Yield (%)[b] |
|---|---|---|
| 1 | $CH_3OH$ | 38 |
| 2 | $CH_3CH_2OH$ | 21 |
| 3 | Cyclohexane | 11 |
| 4 | Toluene | 18 |
| 5 | $CH_3CN$ | 98 |

[a]Reaction conditions: reactant (0.10 mmol), **POMOF 1** (2.1 mol%), Solvent (1.0 mL), r.t., 24 h, LED (10 W), $O_2$. The yield rate was determined by [b]GC. (N-hexadecane was used as the internal

standard substance, Sel.: 99%)

**Table S10.** Quenching experiments to determine the reactive oxygen species (**ROS**) for Photocatalytic Oxidation of Benzylamines. [a]

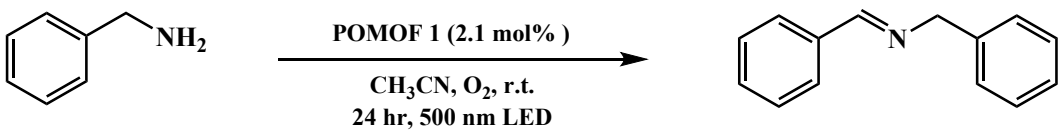


| Entry | trapping reagent | Scavenger | Yield (%)[b] |
|---|---|---|---|
| 1 | 1,4-benzoquinone | $O_2^{\bullet -}$ | 32 |
| 2 | DABCO | $^1O_2$ | 25 |
| 3 | KI | $h^+$ | 19 |
| 4 | $AgNO_3$ | $e^-$ | 21 |
| 5 | isopropanol | $\cdot OH$ | 88 |
| 6 | Standard | --- | 98 |

[a]Reaction conditions: reactant (0.10 mmol), **POMOF 1** (2.1 mol%), $CH_3CN$ (1.0 mL), r.t., 24 h, LED (10 W), $O_2$. The yield rate was determined by [b]GC. (N-hexadecane was used as the internal standard substance, Sel.: 99%)

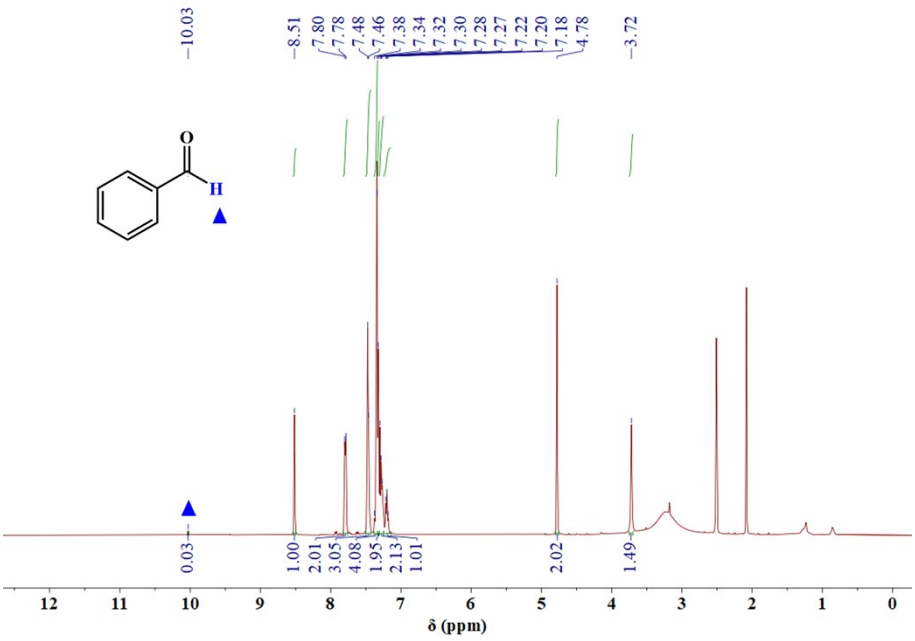


**Figure S28.** $^{1}$H NMR of photocatalytic oxidative coupling of benzylamine at 12 h (small amount of benzaldehyde can be monitored).

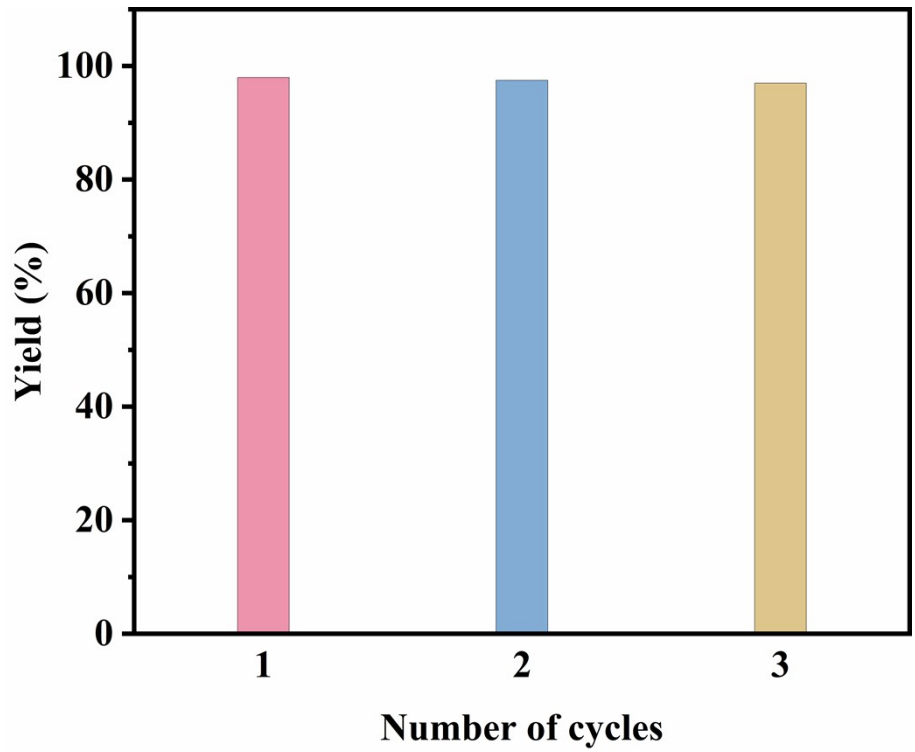


**Figure S29.** Recycling experiments of oxidative benzylamine coupling with **POMOF 1** as photocatalyst.

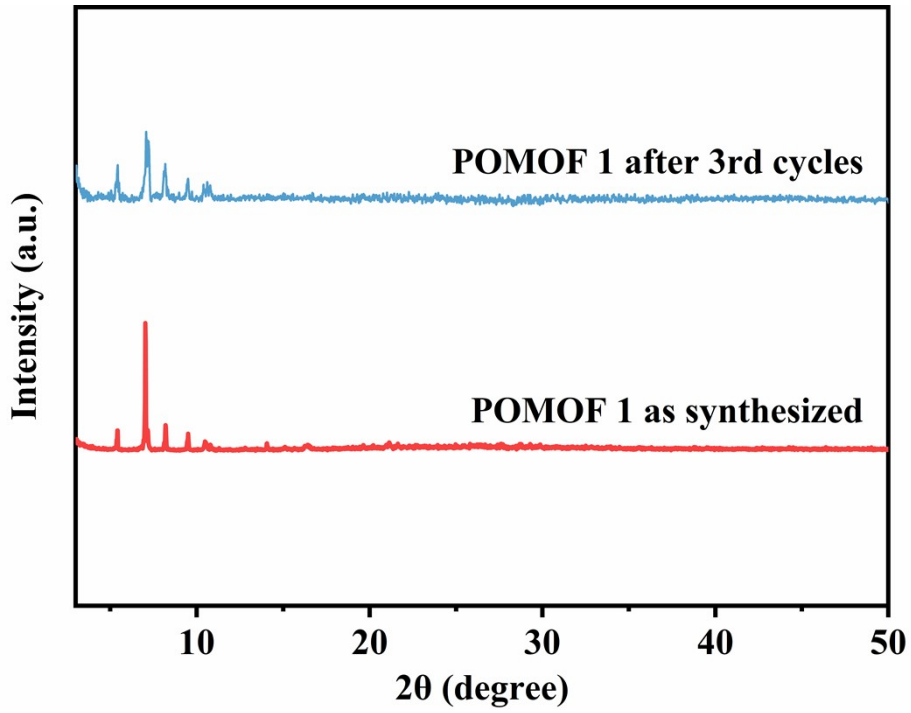


**Figure S30.** Comparison of PXRD patterns of the pristine **POMOF 1** and the recovered **POMOF 1** after three runs of photocatalytic oxidative coupling of benzylamine.

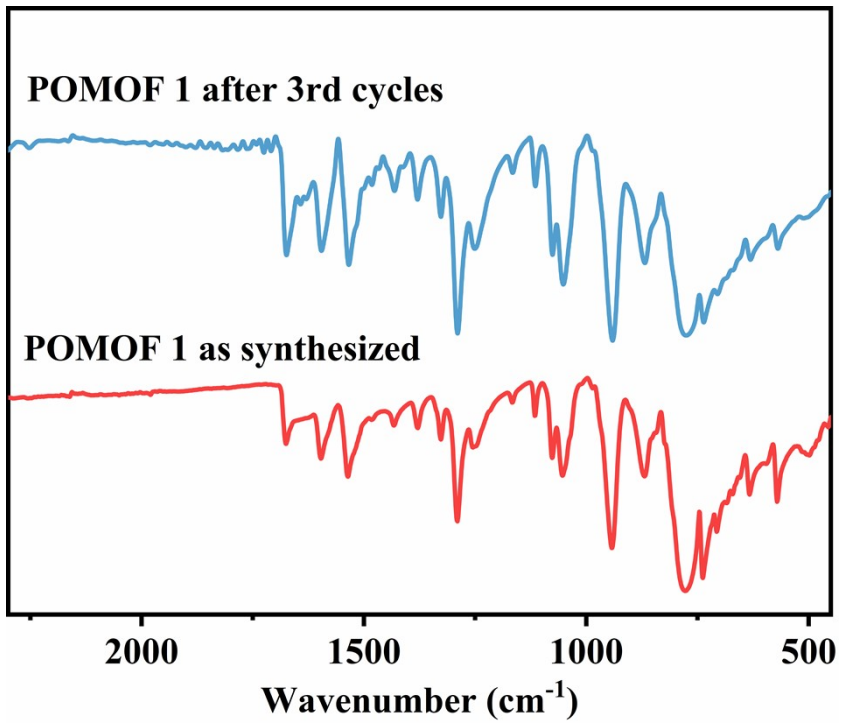


**Figure S31.** Comparison of FT-IR spectra of the pristine **POMOF 1** and the recovered **POMOF 1** after three runs of photocatalytic oxidative coupling of benzylamine.

**Table S11.** ICP Analysis of the mother liquor after filtration of **POMOF 1**.

| Element | Cd | Mo | V |
|---|---|---|---|
| Mother liquor after catalyst filtration (%) | 0.001 | 0.002 | 0.001 |

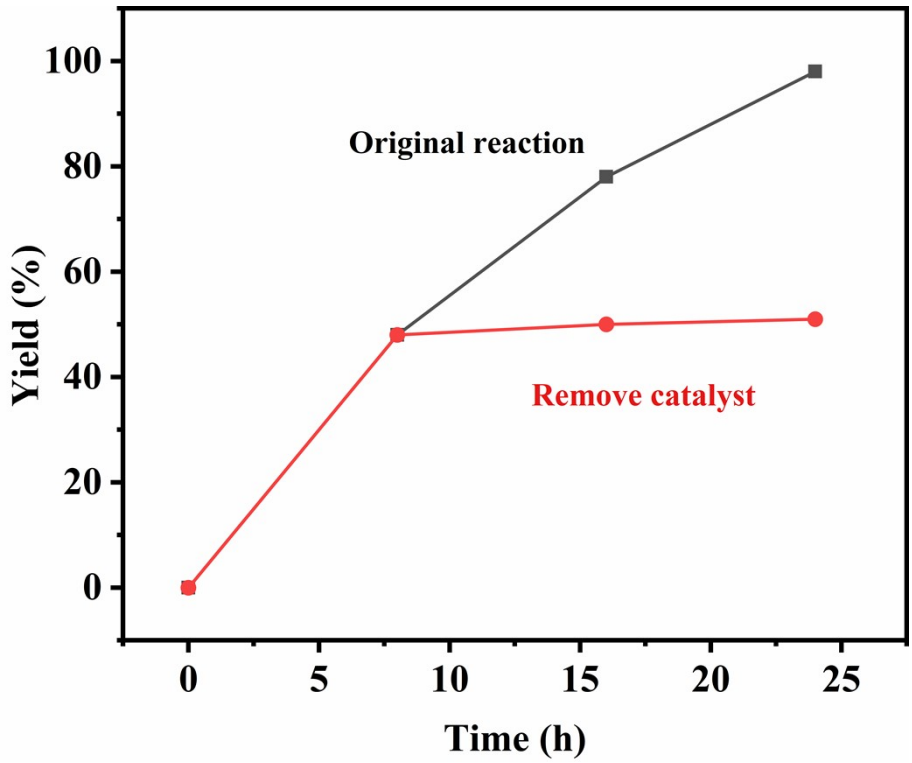


**Figure S32.** Filtration experiment using **POMOF 1** for the photocatalytic oxidative coupling of benzylamine.

**Table S12.** Review on photocatalytic oxidation of benzylamine.

| Catalyst | T (℃) | Light Sourse | Oxidant | t (h) | Yield (%) | Ref. |
|---|---|---|---|---|---|---|
| ZIF-8 | 25 | 450nm LED | $O_2$ | 7 | 3.5 | [4] |
| $Pd_{0.5}$/MTNs | 25 | 400nm LED | air | 12 | 99 | [5] |
| $NH_2$-MIL-125(Ti) | 25 | Blue LED (3W×4) | $O_2$ | 4 | 75* | [6] |
| JNU-207 | 25 | Blue LED | air | 24 | 94 | [7] |
| CF-HCP | 25 | 30W Green LED | $O_2$ | 6 | 91 | [8] |
| Cd-PLA | 25 | 300W Xe lamp | $O_2$ | 6 | 98* | [9] |
| MOF-LS10−12 | 25 | 300W Xe lamp | air | 3 | 94 | [10] |
| 1-Zn | 30 | 465nm LED | air | 2.5 | 98 | [11] |
| B-BO-1,3,5 | 25 | 23W Blue LED | $O_2$ | 24 | 99* | [12] |
| Ti-PMOF-DMA | 25 | Red LED | air | 0.7 | 94* | [13] |
| Py-sp2c-COF | 25 | Green LED | air | 1.8 | 95* | [14] |
| NMNs | 25 | 300W Xe lamp | $O_2$ | 4 | 91 | [15] |
| FJI-Y10 | 40 | 300W Xe lamp | $O_2$ | 6 | 100 | [16] |
| POMOF 1 | 25 | 10W 500 nm LED | $O_2$ | 24 | 98 | This work |
| POMOF 2 | 25 | 10W 500nm LED | $O_2$ | 24 | 76 | This work |
| POMOF 3 | 25 | 10W 500 nm LED | $O_2$ | 24 | 23 | This work |

* The result represented by is conversion rate.

## 7. $^1$H NMR spectrum of photocatalytic oxidation products

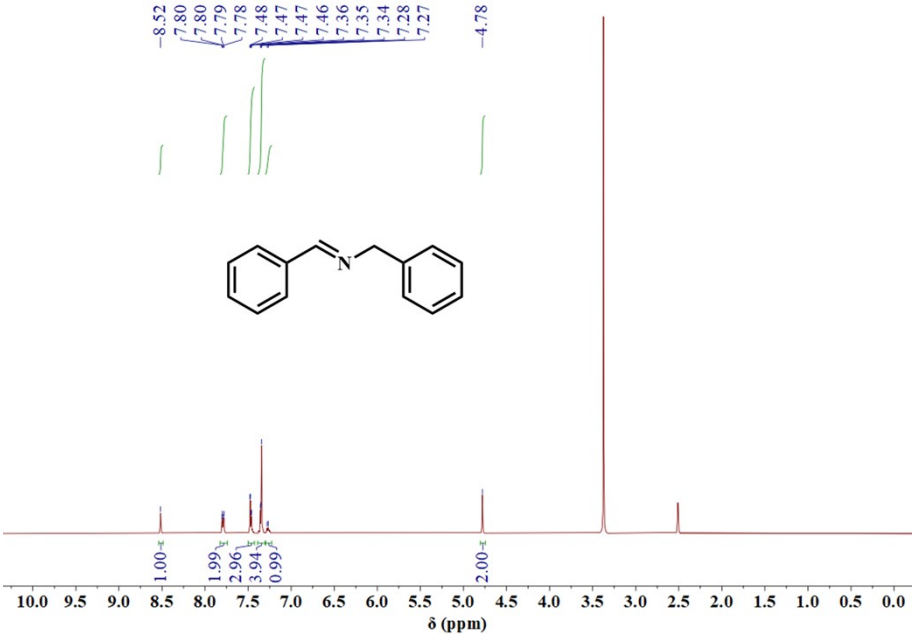


**Figure S33.** The $^1$H NMR (400 MHz, DMSO-$d_6$, ppm) spectrum for the **N-benzylidenebenzylamine**: Yellow oil. δ 8.52 (s, 1H), 7.80 - 7.78 (m, 2H), 7.47 (dd, J = 5.2, 1.9 Hz, 3H), 7.35 (d, J = 4.5 Hz, 4H), 7.28 (d, J = 4.5 Hz, 1H), 4.78 (s, 2H).

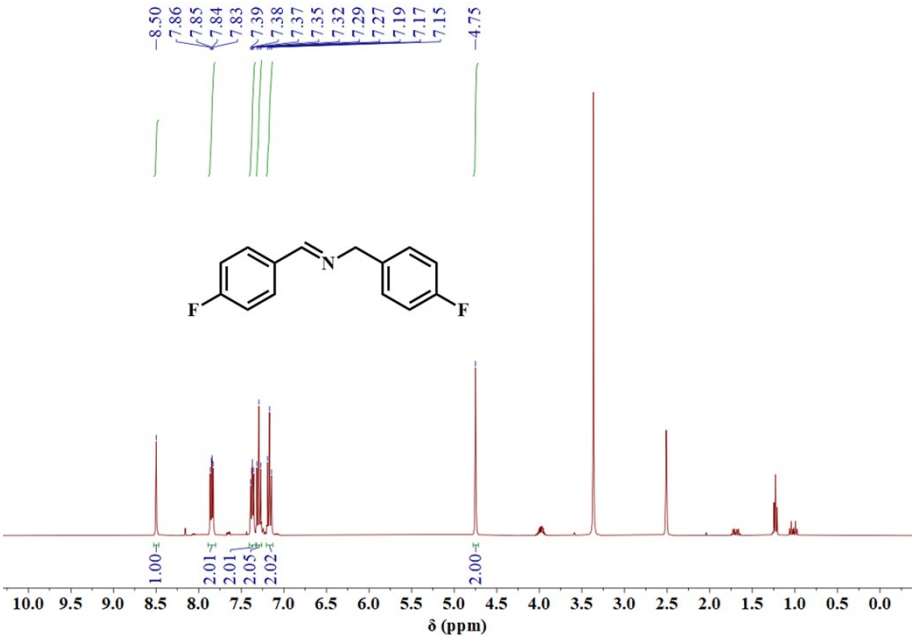


**Figure S34.** The $^1$H NMR (400 MHz, DMSO-$d_6$, ppm) spectrum for the **N-(4-fluorobenzyl)-1-(4-fluorophenyl) methanimine**: Yellow oil. δ 8.50 (s, 1H), 7.86 - 7.83 (m, 2H), 7.37 (dd, J = 8.5, 5.7 Hz, 2H), 7.27 (t, J = 8.8 Hz, 2H), 7.15 (dd, J = 12.4, 5.4 Hz, 2H), 4.75 (s, 2H).

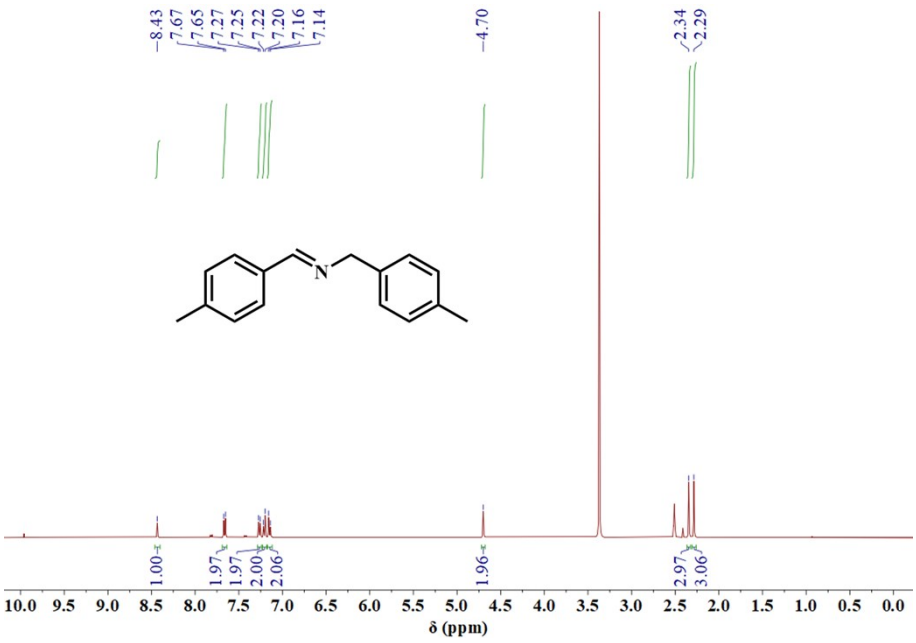


**Figure S35.** The $^{1}$H NMR (400 MHz, DMSO-$d_6$, ppm) spectrum for the **N-(4-methylbenzylidene)-1-(p-tolyl) methanamine**: White solid. δ 8.43 (s, 1H), 7.65 (d, J = 8.0 Hz, 2H), 7.22 (dd, J = 23.4, 7.9 Hz, 4H), 7.14 (d, J = 7.9 Hz, 2H), 4.70 (s, 2H), 2.34 (s, 3H), 2.29 (s, 3H).

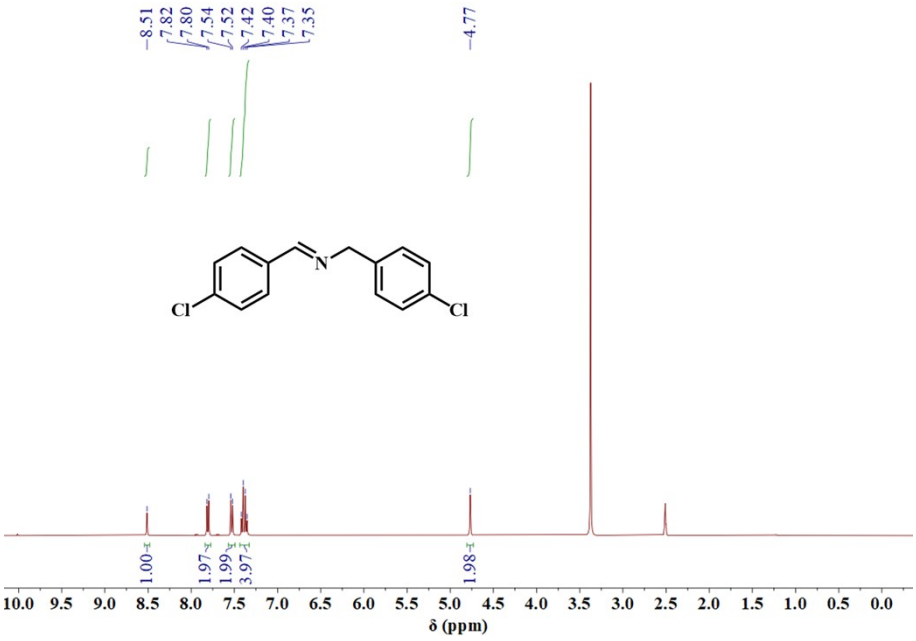


**Figure S36.** The $^{1}$H NMR (400 MHz, DMSO-$d_6$, ppm) spectrum for the **N-(4-chlorphenyl)-1-(4-chlorphenyl) methanimine**: Yellow oil. δ 8.51 (s, 1H), 7.80 (d, J = 8.5 Hz, 2H), 7.52 (d, J = 8.5 Hz, 2H), 7.42 - 7.35 (m, 4H), 4.77 (s, 2H).

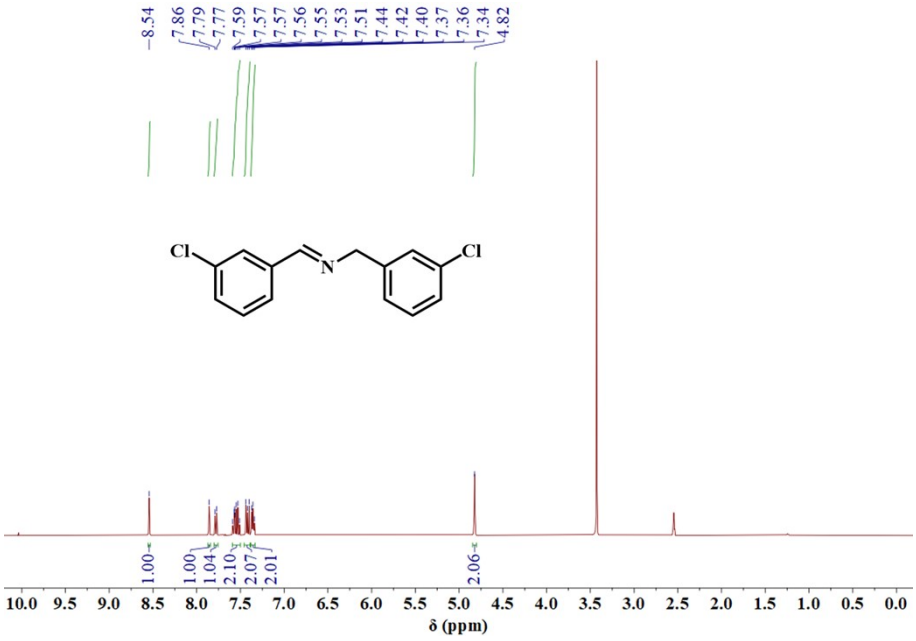


**Figure S37.** The $^{1}$H NMR (400 MHz, DMSO-$d_6$, ppm) spectrum for the **N-(3-chlorphenyl)-1-(3-chlorphenyl) methanimine**: Yellow oil. δ 8.54 (s, 1H), 7.86-7.77 (d, J = 8.5 Hz, 2H), 7.55 (d, J = 8.5 Hz, 2H), 7.44 - 7.34 (m, 4H), 4.82 (s, 2H).

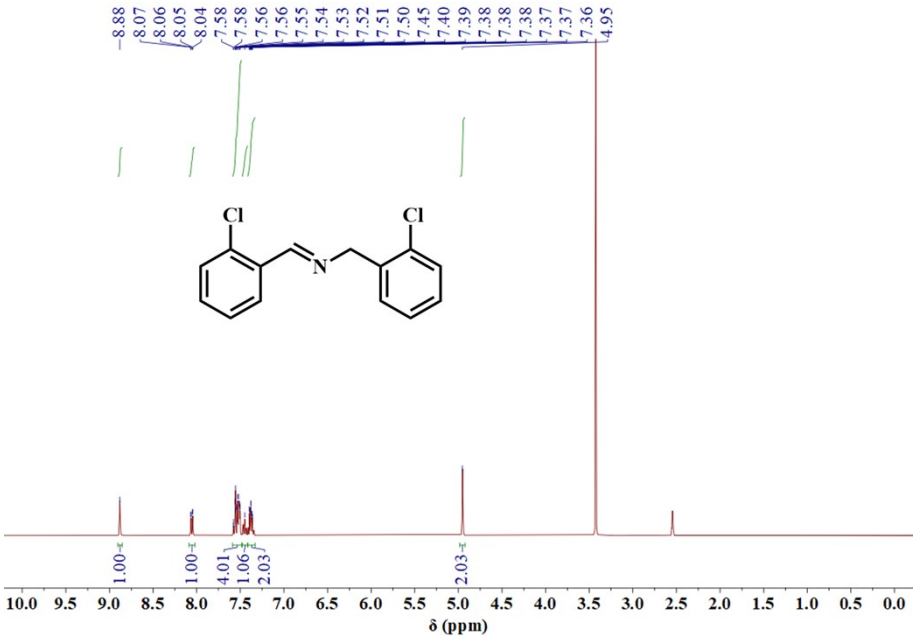


**Figure S38.** The $^{1}$H NMR (400 MHz, DMSO-$d_6$, ppm) spectrum for the **N-(2-chlorphenyl)-1-(2-chlorphenyl) methanimine**: Yellow oil. δ 8.88 (s, 1H), 8.05 (s, 1H), 7.58-7.36 (m, 7H), 4.95 (s, 2H).

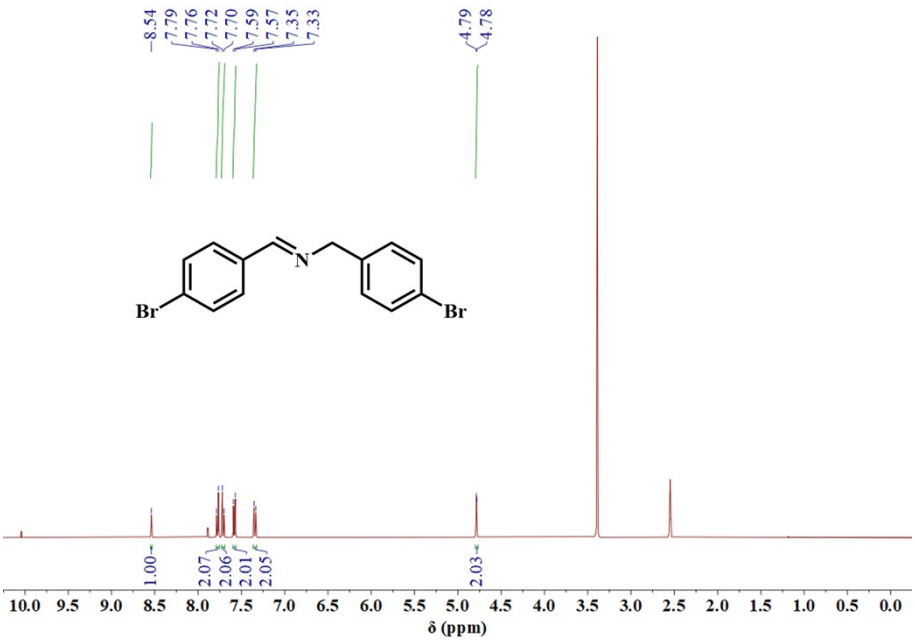


**Figure S39.** The $^{1}$H NMR (400 MHz, DMSO-$d_6$, ppm) spectrum for the **N-(4-bromobenzyl)-1-(4-bromophenyl) methanimine**: Yellow oil. δ 8.54 (s, 1H), 7.76 (d, J = 8.5 Hz, 2H), 7.70 (d, J = 8.4 Hz, 2H), 7.57 (d, J = 8.4 Hz, 2H), 7.33 (d, J = 8.3 Hz, 2H), 4.78 (s, 2H).

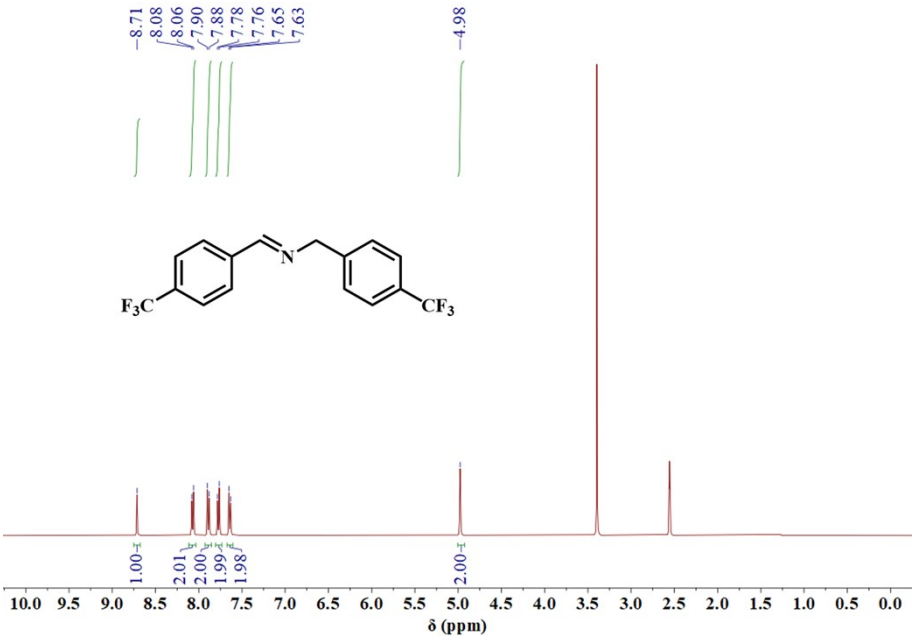


**Figure S40.** The $^{1}$H NMR (400 MHz, DMSO-$d_6$, ppm) spectrum for the **N-(4-(trifluoromethyl) benzyl)-1-(4-(trifluoromethyl)phenyl) methanimine**: Yellow oil. δ 8.71 (s, 1H), 8.06 (m, 2H), 7.88 (dd, J = 8.5, 5.7 Hz, 2H), 7.76 (t, J = 8.8 Hz, 2H), 7.63 (dd, J = 12.4, 5.4 Hz, 2H), 4.98 (s, 2H).

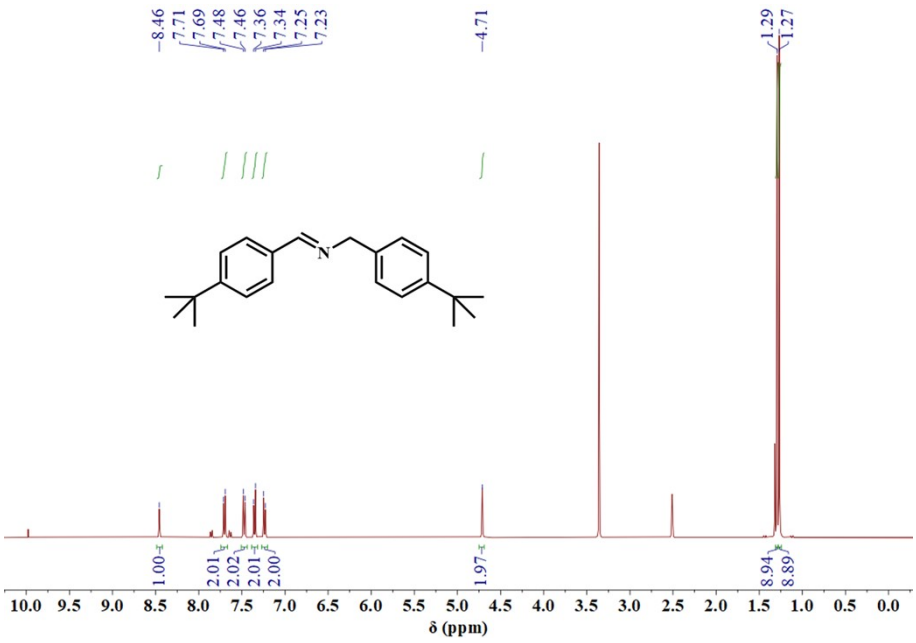


**Figure S41.** The $^{1}$H NMR (400 MHz, DMSO-$d_6$, ppm) spectrum for the **N-( (4-butylbenzyl)-1-(4-butylbenzyl) methanamine**: Yellow oil. δ 8.46 (s, 1H), 7.69 (d, J = 8.0 Hz, 2H), 7.46 (d, 2H), 7.34 (d, 2H), 7.23 (d, 2H), 4.71 (s, 2H), 1.29 (m, 9H), 1.27 (m, 9H).

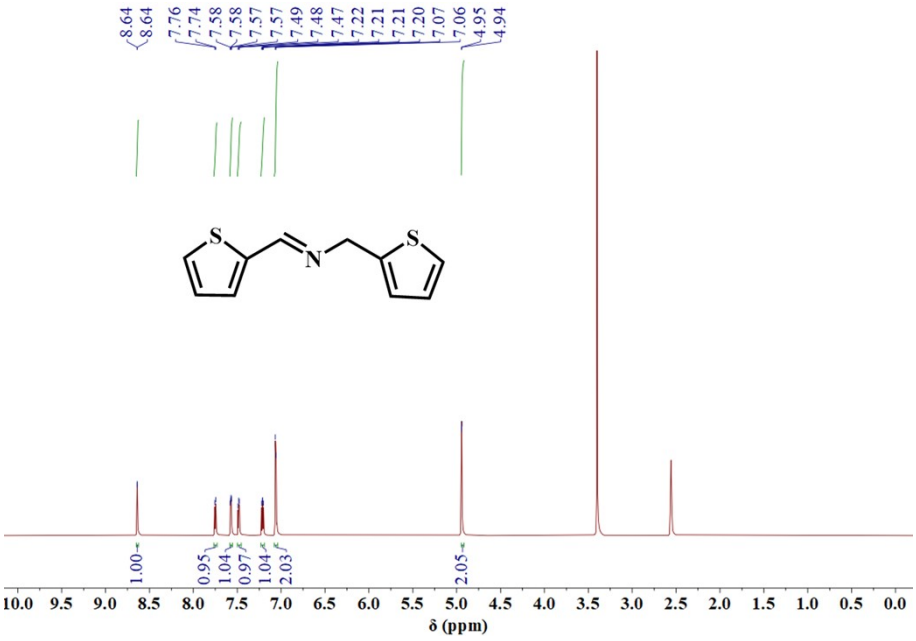


**Figure S42.** The $^{1}$H NMR (400 MHz, DMSO-$d_6$, ppm) spectrum for the **1-(thiophen-2-yl)-N-(thioph en-2-ylmethyl) methanimine**: Yellow oil. δ 8.64 (d, J = 1.1 Hz, 1H), 7.74 (m, 1H), 7.57 (dd, J = 3.6, 1.0 Hz, 1H), 7.47 (dd, J = 4.0, 2.4 Hz, 1H), 7.21 (dd, J = 5.0, 3.6 Hz, 1H), 7.06 (m, 2H), 4.94 (d, J = 0.8 Hz, 2H).

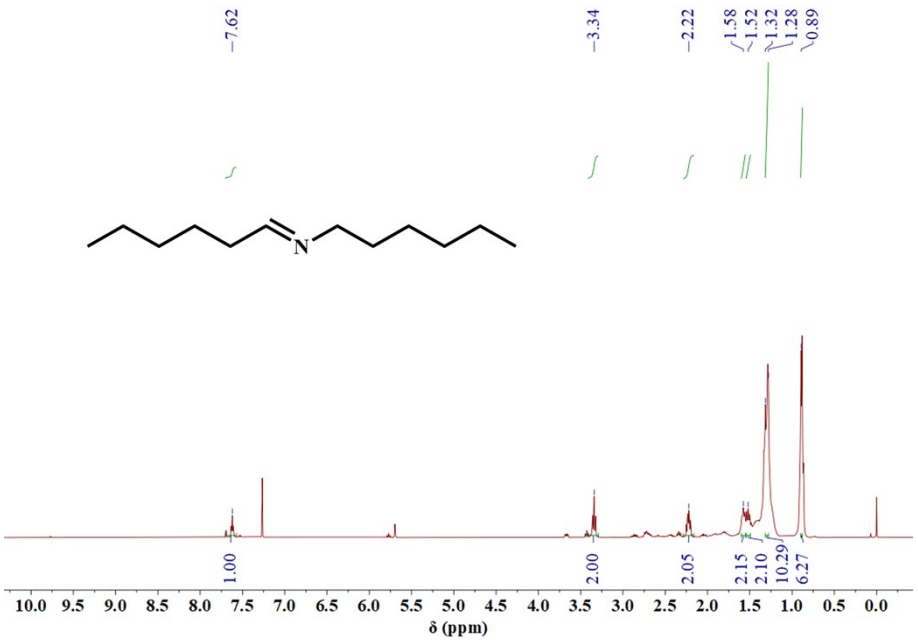


**Figure S43.** The $^{1}$H NMR (400 MHz, Chloroform-*d*, ppm) spectrum for the **(E)-N-hexylhexan-1-imine**: Yellow oil.δ 7.62 (m, 1H), 3.34 (dt, J = 33.9, 7.0 Hz, 2H), 2.22 (m, 2H), 1.58 (m, 2H), 1.52 (s, 2H), 1.32 − 1.28 (t, J = 3.5 Hz, 10H), 0.89 (d, J = 4.3 Hz, 6H).

## 8. References


1. H.-R. Tan, X. Zhou, T. Gong, H. You, Q. Zheng, S.-Y. Zhao and W. Xuan, *RSC Adv.*, 2024, **14**, 364-372.
2. H. Wang, M. Zhao, Q. Zhao, Y. Yang, C. Wang and Y. Wang, *Ind. Eng. Chem. Res.*, 2017, **56**, 2711-2721.
3. R. Tayebee and S. Tizabi, *Chin. J. Catal.*, 2012, **33**, 962-969.
4. Z. X. Sun, K. Sun, M. L. Gao, Ö. Metin and H. L. Jiang, *Angew. Chem., Int. Ed.*, 2022, **134**, e202206108.
5. H. Wang, J. Yu, S. Wei, M. Lin, Y. Song and L. Wu, *Chem. Eng. J.*, 2022, **441**, 136020.
6. W. Sheng, F. Huang and X. Lang, *Mater. Today Chem.*, 2023, **30**, 101505.
7. K. Wu, J.-K. Jin, X.-Y. Liu, Y.-L. Huang, P.-W. Cheng, M. Xie, J. Zheng, W. Lu and D. Li, *J. Mater. Chem. C*, 2022, **10**, 11967-11974.
8. Y. Zhi, K. Li, H. Xia, M. Xue, Y. Mu and X. Liu, *J. Mater. Chem. A*, 2017, **5**, 8697-8704.
9. D. Wang, C. Sun and Y. Wang, *Eur. J. Inorg. Chem.*, 2024, **27**, e202300575.
10. B. Ge, Y. Ye, Y. Yan, H. Luo, Y. Chen, X. Meng, X. Song and Z. Liang, *Inorg. Chem.*, 2023,

**62**, 19288-19297.
11. Q.-Q. Li, P.-H. Pan, H. Liu, L. Zhou, S.-Y. Zhao, B. Deng, Y.-J. He, J.-X. Song, P. Liu, Y.-Y. Wang and J.-L. Li, *Inorg. Chem.*, 2023, **62**, 17182-17190.
12. Z. J. Wang, S. Ghasimi, K. Landfester and K. A. I. Zhang, *Adv. Mater.*, 2015, **27**, 6265-6270.
13. W. Sheng, F. Huang, X. Dong and X. Lang, *J. Colloid Interface Sci.*, 2022, **628**, 784-793.
14. H. Hao, F. Zhang, X. Wang, F. Huang, S. Chen and X. Lang, *Adv. Funct. Mater.*, 2024, 2419735.
15. T. Wu, Y. Shi, Z. Wang, C. Liu, J. Bi, Y. Yu and L. Wu, *ACS Appl. Mater. Interfaces*, 2021, **13**, 61286-61295.
16. F.-J. Zhao, G. Zhang, Z. Ju, Y.-X. Tan and D. Yuan, *Inorg. Chem.*, 2020, **59**, 3297-3303.